MULTISCALE MODEL. SIMUL.
Vol. 3, No. 3, pp. 629–657

MODELING OF ISLAND FORMATION DURING SUBMONOLAYER DEPOSITION: A STOCHASTIC GEOMETRY-BASED SIMULATION APPROACH*

MAOZHI LI† AND J. W. EVANS‡

Abstract. Homogeneous nucleation and growth of two-dimensional islands during submonolayer deposition has been analyzed extensively by kinetic Monte Carlo (KMC) simulation of atomistic models and more recently by Burton–Cabrera–Frank-type continuum formulations for diffusion and aggregation of the deposited adatoms. Here, we develop an alternative geometry-based simulation (GBS) approach. This approach replaces an explicit treatment of adatom diffusion (either within an atomistic or continuum framework) with a formulation based on the stochastic geometry of "depletion zones" or "capture zones" surrounding islands. We consider models with a prescribed critical size, i, above which islands are stable. For canonical models with small i, we show that prediction of the nucleation rate and island density by GBS (or any other multiscale approach) requires precise description of adatom capture by critical clusters, for which we extend existing theory. We also present results for the island size distribution including the regime of large i where KMC simulation becomes inefficient and where the initial transient regime of the growing adatom population becomes protracted and thus more important. Finally, we discuss extension of the GBS approach to treat island coalescence and multilayer growth, and to a variety of other nucleation mechanisms.

Key words. epitaxial growth, island formation, Monte Carlo simulation, diffusion, aggregation, capture zone

AMS subject classifications. 35Q99, 35R35

DOI. 10.1137/040606569

1. Introduction.

Deposition processes on perfect atomically flat crystalline surfaces are of interest both from the perspective of fundamental science and due to numerous important technological applications [1, 2]. In these processes, atoms are deposited at random at a periodic array of adsorption sites at flux F, with units of atoms per site per unit time, or, equivalently, monolayers (ML) per unit time. Thereafter, adsorbed atoms (adatoms) hop between adjacent sites, at rate h (per direction), nucleating new stable immobile islands, when sufficient numbers of diffusing adatoms meet, and aggregating with existing stable immobile islands. Thus, the overall process involves a competition between diffusion-mediated nucleation of new islands and growth of existing islands. Traditionally, the concept of a critical size, i, was introduced, such that only clusters of more than i atoms are stable. Thus, nucleation of a stable island occurs when a diffusing adatom reaches a critical cluster of i atoms. Precise treatment of these problems, even for the simplest case of irreversible island formation ($i = 1$), constitutes a fundamental challenge in the analysis of far-from-equilibrium phenomena, akin to analysis of Ising-type models for equilibrium systems.

*Received by the editors April 9, 2004; accepted for publication (in revised form) July 22, 2004; published electronically March 3, 2005. This work was supported by NSF grant CHE-0414378. It was performed at Ames Laboratory, which is operated for the U.S. Department of Energy by Iowa State University under contract W-7405-Eng-82.

http://www.siam.org/journals/mms/3-3/60656.html

†Institute of Physical Research and Technology and Ames Laboratory-USDOE, Iowa State University, Ames, IA 50011 (maozhi@scl.ameslab.gov).

‡Department of Mathematics and Ames Laboratory-USDOE, Iowa State University, Ames, IA 50011 (evans@ameslab.gov).

The traditional mean-field rate equation formulation of these problems was developed in the 1960s by Zinsmeister [3], Venables [4], et al. This formulation proved valuable for assessing behavior of mean density (per site) of stable islands, N_{isl}. In the 1990s, precise kinetic Monte Carlo (KMC) simulation studies of atomistic deposition models revealed failure of mean-field predictions for island size distribution [5, 6, 7, 8]. Only later was this failure identified as resulting from a subtle correlation between island size and separation [9]. This feature was ignored in mean-field treatments, which assume that the local environment of an island is independent of its size. Specifically, it was shown that larger islands are further separated from their neighbors, which implies that they have larger surrounding "capture zones" (CZs) for depositing atoms [9].

While KMC simulation is very effective for small i, it becomes inefficient for highly reversible island formation (large i) due to the much higher density (per site) of diffusing atoms, N_1. Thus, it is appropriate to consider alternative approaches. Since the characteristic separation between islands is often large, it is natural to replace the atomistic description of deposition, diffusion, and aggregation with a continuum partial differential equation (PDE)-based formulation for N_1 [10, 11, 12, 13, 14, 15, 16, 17, 18, 19, 20, 21]. Bartelt et al. [10, 11] confirmed the utility and validity of this Burton–Cabrera–Frank (BCF)-type approach [22] as applied to island formation during deposition. Furthermore, Bartelt et al. [10, 11] provided an exact construction of CZs surrounding islands [9, 10, 11, 23, 24], so that the rate of growth of an island (reflecting the total diffusive flux of adatoms at its edge) was given exactly in terms of its CZ area. To simulate the overall island formation process for both submonolayer and multilayer regimes, one popular strategy is to combine this BCF-type formulation with (i) a classical prescription of island nucleation [4] at a rate or probability proportional to the local value of $(N_1)^{i+1}$ and (ii) a continuum treatment of the evolution of island edges (island dynamics). Level-set formulations [12, 13, 14, 15, 16] provide an example of the latter.

One significant outstanding challenge with such continuum formulations is the appropriate treatment of island edge dynamics, which is determined by both aggregation and relaxation processes. In the initial stages of island growth, most aggregating adatoms arrive at the island edge from the region exterior to the island (after diffusing across the substrate), rather than from the region interior to the island (after landing on top). The effect of the former is to produce a diffusion-limited-aggregation (DLA)- or Mullins–Sekerka-type instability in the shape of the growing island [25], which dominates the anti-DLA stabilizing effect of on-top deposition [26]. This instability has also been studied extensively in the context of Laplacian growth [27]. Also, for roughly straight steps on a vicinal surface, the presence of an additional activation barrier or reduced hopping rate for downward transport produces an analogous Bales–Zangwill instability [28] due to dominant attachment from the lower terrace. In physical deposition studies, this island shape instability is often quenched by relaxation processes such as periphery diffusion at island edges, since these relaxation processes are fairly efficient except at low temperatures.

However, in existing level-set treatments nominally without periphery diffusion, the island shape instability usually does not develop before island coalescence [12, 13, 14, 15, 16]. Here, quenching of the shape instability derives artificially from the numerical method (finite grid size, etc.). Thus, to reliably describe irregular fractal or dendritic island shapes which can arise from the DLA instability at lower temperatures (due to limited shape relaxation), further development is needed. One strategy for treating fluctuation and shape instability effects at lower temperatures is to adopt a

hybrid approach. Here, the island edge and its dynamics are treated in an atomistic framework but terrace diffusion is described within a continuum framework [29, 30]. However, it should be noted that shape instability is usually observed in experiments only at lower temperatures corresponding to irreversible (or weakly reversible) island formation with small i. Thus, in general, one expects that a conventional KMC simulation of an atomistic model will provide the most efficient and realistic treatment of such systems.

Perhaps of more significance for multiscale modeling is the regime of higher temperatures with significant island shape relaxation, where fluctuations in island growth are typically quenched and islands have compact but nonequilibrium growth shapes. Here, it is reasonable to maintain a fully continuum treatment. However, for level-set or any other multiscale formulation to appropriately describe any specific physical system, it is essential to incorporate a realistic treatment of these compact nonequilibrium island growth shapes. Unfortunately, appropriate treatment of shape relaxation via the "simplest" mechanism of periphery diffusion of adatoms along island edges is nontrivial. Although the traditional Mullins near-equilibrium expression for the diffusive flux of atoms along the step edge (or a simplification thereof) is often adopted by default [16, 21, 31], this is not necessarily valid for island growth during deposition [32]. During growth, nonequilibrium diffusive fluxes along the step edge can dominate the equilibrium Mullins flux. One recent study derived appropriate continuum expressions for these fluxes in a simple model and then applied them to an analysis of island growth coalescence shapes [32]. Reliable treatment of island coalescence is a key component of effective simulation of film growth above ~ 0.3 ML.

The above BCF-type approaches require a computationally demanding solution of a boundary value problem for a deposition-diffusion equation in a complex many-island geometry. Except for the initial "transient regime" of deposition, it suffices to treat a time-independent problem for the "steady-state" regime [4], where there is a rough balance between the gain of adatoms due to deposition and their loss due to aggregation with "slowly" growing islands. However, even this steady-state boundary value problem is computationally demanding. Thus, to circumvent analysis of this problem, we have developed an alternative approach termed *geometry-based simulation* (GBS) in which we reformulate the problem within the framework of stochastic geometry rather than PDEs [33, 34]. In the transient regime, the key feature is the specification of nucleation as occurring outside depletion zones (DZs), i.e., regions where N_1 is depleted, which expand about just-nucleated islands. In the steady-state regime, the entire surface is tessellated into CZs surrounding each island, and *both* island nucleation and growth are prescribed in terms of this tessellation. Preliminary analysis reveals that this approach is successful in correctly predicting detailed features of the island distribution, e.g., island size and CZ area distributions, as well as island spatial correlations [33, 34].

To highlight and contrast the difference between BCF- and GBS-based treatment, we provide the following further comments. In BCF, one solves the boundary value problem for N_1 and implements nucleation at rate $\propto (N_1)^{i+1}$. In GBS, we *approximate* the diffusion field N_1 as constant outside suitably chosen DZs and by using a circularly symmetric steady-state approximation inside CZs. The nucleation rate is then calculated by the same formula as for BCF. However, nucleation positions are chosen randomly outside DZs (where N_1 is spatially uniform) in the transient regime or near the CZ boundaries (where N_1 is relatively large) in the steady-state regime.

In BCF, island growth is determined from the diffusion flux at island edges, which is again determined from solving the boundary value problem for N_1. In GBS,

island growth in the transient regime is determined by analyzing the time-dependent deposition-diffusion equation for growth of a single isolated island. In the steady-state regime, it is determined from the area of the CZ, which is approximated by a simple but effective geometric construction. A more detailed description of the implementation of GBS will be provided in the following sections.

In this paper, we further develop and test this GBS approach for canonical deposition models with small critical size, i. We also extend GBS to treat the regime of large i, as well as discussing its application to a variety of other nucleation mechanisms. The mean-field rate equation and GBS formulations are reviewed in section 2, where we also present new formulations for key quantities related to nucleation. The focus of this paper is on lower submonolayer coverages, where island coalescence is not significant. In any multiscale study of island formation during deposition, a precise characterization of the nucleation rate is essential. Thus, in section 3, we present a detailed discussion of the capture number for critical clusters, which controls this rate. Then, in section 4, we present a detailed analysis of canonical models for small critical size comparing results of GBS studies with exact KMC simulation studies. We also clarify the persistence and dominance of nucleation in the steady-state regime, a rarely appreciated feature of these processes. Next, in section 5, we treat the regime of large critical size (i.e., highly reversible island formation) pursuing an often stated goal of applying multiscale modeling approaches to these problems. This requires a refined treatment of the transient regime (which becomes protracted and thus more significant for large i) and leads to the first non-mean-field results for the island size distribution. Next, in section 6, we discuss extensions of the GBS approach to treat the island coalescence regime (exploiting the concept of sub-CZs for each island edge) and also multilayer growth in the presence of an Ehrlich–Schwoebel (step-edge) barrier inhibiting downward transport [35, 36]. Finally, in section 7, we discuss the extension of GBS to treat other mechanisms for island nucleation and growth. Conclusions are provided in section 8.

2. Rate equation and GBS formulations. The following analyses apply to atomistic models for island nucleation and growth during deposition with a prescribed critical size, i. The key atomistic steps are described in section 1: random deposition at rate F per site on a square lattice of adsorption sites; diffusive hopping of isolated adatoms to adjacent sites at rate h; and aggregation into islands which are stable and immobile when containing more than i adatoms (i.e., adatoms cannot detach from such islands). Since nucleation occurs when a diffusing adatom reaches a critical cluster of i adatoms (or when an atom is deposited next to such a cluster), the density of such critical clusters is a key determinant of the nucleation rate. This in turn is strongly dependent on the binding energy, $E_i \leq 0$, for such critical clusters, as discussed below [4]. Thus nucleation is irreversible for $i = 1$ (where $E_1 = 0$) and reversible for $i > 1$ (where a smaller magnitude of E_i implies greater difficulty in nucleating stable clusters, and thus greater reversibility).

In addition, in our modeling, we consider the case where individual growing islands can readily achieve a near-square quasi-equilibrium shape due to efficient edge diffusion of aggregating atoms [6]. This choice mimics metal(100) homoepitaxy [1, 7, 37]. Further, we assume that atoms deposited on top of islands readily hop down at the edge of islands, and thus contribute to island growth, rather than nucleating new islands in the second layer [6].

2.1. Mean-field rate equation analysis. From an approximate rate equation formulation for mean densities (per site) of diffusing adatoms, N_1, and of islands, N_{isl},

in the above models, one can extract key insight into various stages of nucleation and growth. (In section 2.1, N_1 will denote the spatial average of the adatom density, whereas in section 2.2, it will denote a local value depending on position.) First, define the capture number for critical islands, σ_i, which appears in the nucleation rate, $K_{nuc} = \sigma_i h N_1 N_i$, and the mean capture number for stable islands, σ_{av}, which appears in the aggregation rate, $K_{agg} = \sigma_{av} h N_1 N_{isl}$. Here, N_i is the mean density of critical clusters of i adatoms which is assumed to satisfy the quasi-equilibrium Walton relation,

$$N_i \approx c_i \exp[-\beta E_i](N_1)^i, \tag{2.1}$$

where $\beta = 1/(k_B T)$ is the inverse temperature [4]. For small coverage $\theta = Ft$, one has [4]

$$\frac{dN_1}{dt} \approx F - (i+1)K_{nuc} - K_{agg}, \quad \text{and} \quad \frac{dN_{isl}}{dt} \approx K_{nuc}. \tag{2.2}$$

Integration of (2.2) reveals a transient regime where initially $N_1 \sim Ft = \theta$, followed by crossover at

$$\theta \sim \theta^* \sim \exp[\beta E_i/(i+3)](h/F)^{-2/(i+3)} \tag{2.3}$$

to a steady-state regime where $dN_1/dt \approx F - K_{agg} \approx 0$. The latter implies the steady-state relation $N_1 \approx F/(\sigma_{av} h N_{isl})$. One finds that the mean island density satisfies

$$N_{isl} \approx (i+2)^{-1} c_i \sigma_i \theta^{i+2} \exp[-\beta E_i](h/F) \qquad \text{in the transient regime,} \tag{2.4a}$$

$$N^*_{isl} \sim (i+2)^{-1} \exp[-\beta E_i/(i+3)](h/F)^{-\chi^*} \qquad \text{at crossover } \theta^*, \tag{2.4b}$$

$$N_{isl} \sim \theta^{1/(i+2)} \exp[-\beta E_i/(i+2)](h/F)^{-\chi} \quad \text{in the steady-state regime.} \tag{2.4c}$$

The scaling exponents satisfy $\chi = i/(i+2)$ and $\chi^* = (i+1)/(i+3)$, so $\chi^* - \chi = 2(i+2)^{-1}(i+3)^{-1} > 0$. We also note that the coverage dependence in (2.4c) is modified for $\theta = \mathrm{O}(1)$ due to the θ-dependence of the capture numbers and due to other factors not included in this simple analysis.

Of particular significance in this study is the behavior of the nucleation rate. After a natural rescaling, $\tilde{K}_{nuc} = K_{nuc}/F = c_i \sigma_i (h/F) \exp[-\beta E_i](N_1)^{i+1}$, this rate can be written as

$$\tilde{K}_{nuc} \sim c_i \sigma_i (h/F)^{-(i-1)/(i+3)} \exp[-2\beta E_i/(i+3)](\theta/\theta^*)^q, \tag{2.5}$$

where the exponent q satisfies $q = i+1$ in the transient regime, and $q = -(i+1)/(i+2)$ in the steady-state regime. This behavior corresponds to a dramatic increase in nucleation as θ approaches θ^* from below (especially for large i), followed by a slower decrease above θ^*, with the maximum rate occurring at around θ^*. Finally, it is also appropriate to comment on behavior of the mean island size (measured in atoms), S_{av}. The amount of material incorporated into stable growing islands is given by $\theta_{grow} = \int_0^t dt' K_{agg}(t')$, so it follows that $S_{av} = \theta_{grow}/N_{isl}$. One finds that $\theta^*_{grow} \approx \theta^*/i^2$ at crossover θ^*, and $\theta_{grow} \approx \theta$ for $\theta = \mathrm{O}(1)$. It thus follows that

$$S^*_{av} \sim i^{-1} \exp[2\beta E_i/(i+3)](h/F)^{(i-1)/(i+3)} \quad \text{at crossover } \theta^*, \quad \text{and} \tag{2.6a}$$

$$S_{av} \sim \exp[\beta E_i/(i+2)](h/F)^{i/(i+2)} \qquad \text{in the steady-state regime.} \tag{2.6b}$$

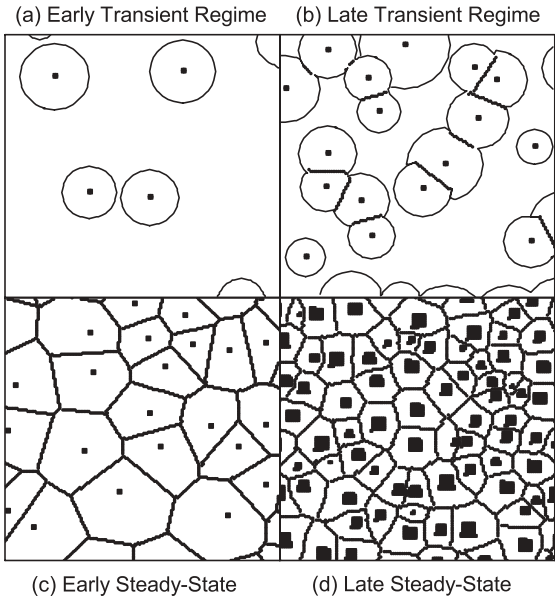

FIG. 2.1. *Schematic of island formation during deposition.* (a) *Expansion of nonoverlapping depletion zones (DZs) early in the transient regime.* (b) *Further expansion and collision of DZs later in the transient regime.* (c) *Tessellation of the surface by "large" capture zones (CZs) early in the steady-state regime.* (d) *Tessellation of the surface into smaller CZs later in the steady-state regime after subsequent significant nucleation. Configurations were generated from GBS for* $i = 1$ *with* $h/F = 10^6$. *The images show a region of* 150×150 *lattice sites.*

The results (2.4a) and (2.4c) for transient and steady-state behavior are well known [4], but the consequences of these results and the subsequent results (2.5) and (2.6) are not well known or appreciated. We discuss some key consequences for two separate regimes of i:

(i) Small critical sizes ($i = 1, 2, 3, \dots$). Since $\chi^* - \chi > 0$ is not negligible, the steady-state N_{isl} far exceeds the crossover value N^*_{isl}. Consequently, for typical $h/F = 10^6 - 10^{10}$, most nucleation occurs in the steady-state regime. Also, since S^*_{av} is far below S_{av}, island growth up to crossover is "negligible." In the most extreme case, one has that $S^*_{av} = \mathrm{O}(1)$ for $i = 1$.

(ii) Large critical sizes ($i \gg 1$). One expects that $E_i \approx i\epsilon$, for large i, where ϵ denotes the amount of bonding per atom. Then, it follows that $N_{isl} \sim \exp[-\beta\epsilon](h/F)^{-1}$ in the steady-state regime, and N^*_{isl} is comparable to N_{isl} (smaller roughly by a factor of i). The same conclusion follows comparing S_{av} in the steady state with S^*_{av}. Thus, nucleation is much more significant in the transient regime (relative to small i), and one cannot neglect island growth in this regime.

2.2. The GBS algorithm. For GBS, essentially we just need to specify the rules for determining island nucleation and growth and then implement these processes with the correct relative rates [33, 34]. We first give a brief overview of our separate algorithms for the transient and steady-state regimes. The following presentation of the GBS algorithm is best illustrated using the schematic in Figure 2.1. This schematic was actually obtained from snapshots of judiciously selected GBS simulations for $i = 1$ and $h/F = 10^6$ to illustrate key features of behavior for small critical size.

(I) In the transient regime, nucleated islands are surrounded by expanding de-

pletion zones (DZs), with radii $R_{DZ}(\delta t) \sim (h\delta t)^{1/2}$, where δt is the time since nucleation. A precise determination of R_{DZ} follows from analysis of the appropriate time-dependent deposition-diffusion equation for N_1 in a circular geometry [4, 8, 34],

(2.7)
$$\frac{dN_1(r,t)}{dt} = F - (i+1)K_{nuc} + h\nabla^2 N_1 = F - (i+1)K_{nuc} + h\frac{1}{r}\frac{\partial}{\partial r}\left(r\frac{\partial}{\partial r}\right)N_1(r,t),$$

with $N_1 = 0$ at the island edge (a sink for diffusing adatoms). The term involving the nucleation rate is determined from $K_{nuc} = c_i\sigma_i h \exp[-\beta E_i](N_1)^{i+1}$. This term should be included for $i = 1$ (refining the treatment in [34]) since associated loss of adatoms is significant, but it is less significant for $i > 1$. Initially, these DZs have no significant overlap. Inside each DZ, aggregation of adatoms with the growing island causes significant depletion of the adatom density, N_1, from its transient "background" value of $N_1 = \theta_-$ determined from solution of $dN_1/dt = F-(i+1)K_{nuc}$. Thus, in our GBS algorithm, we nucleate islands at randomly chosen locations outside the DZs at a uniform rate determined by $N_1 \approx \theta_-$. Consequently, the total nucleation rate per site satisfies

$$K_{nuc}(tot) = c_i\sigma_i h \exp[-\beta E_i](\theta_-)^{i+1}A_{nuc}, \tag{2.8}$$

where A_{nuc} is the area outside the DZs. Approaching crossover, DZs start to overlap, initiating the formation of so-called capture zones (CZs) which are defined explicitly below. In this geometric picture, the significant reduction in A_{nuc} as DZs overlap and cover much of the surface halts the increase of K_{nuc} with θ. This produces a maximum in K_{nuc}, as described in section 2.1, occurring roughly at crossover $\theta \approx \theta^*$. For small i, island growth is not significant in this regime and is thus ignored. Treatment of island growth is necessary for large i, and is described in section 4.

(II) In the subsequent steady-state regime, the adatom density, N_1^{ss}, is determined by a balance between gain due to deposition and loss due to aggregation. We regard the surface as completely covered by CZs (formed by colliding DZs). Ideally, these are constructed from N_1^{ss} so that the "free" CZ area (CZ area less the island area) times F exactly equals the contribution to the island growth rate due to aggregation of adatoms diffusing across the substrate [10]. The total island growth rate, including a contribution deposition on top of islands (determined by their size), then equals the total CZ area times F. Instead of exact construction of CZs based on N_1^{ss}, we use a Voronoi cell-type construction based on the distance from island edges (i.e., any point in a CZ is closer to the edge of its island than to any other island) [11, 33, 34]. Then, the areas of the Voronoi-type cells (rather than the exact CZs) are used to determine the island growth rates, a procedure which has been shown to be reliable [11]. In our GBS algorithm, islands are grown to maintain a near-square shape.

The total nucleation rate is determined by summing over contributions for each CZ,

(2.9)
$$K_{nuc}(tot) = \sum_{CZ} K_{nuc}(CZ), \quad \text{where} \quad K_{nuc}(CZ) = c_i\sigma_i h \exp[-\beta E_i]\int_{CZ} dA(N_1^{ss})^{i+1}.$$

Here $K_{nuc}(CZ)$ is estimated in terms of the CZ area, A, and the size of the associated island size, s, using a circular-geometry approximation for N_1^{ss}. Specifically, we solve the steady-state version of the deposition-diffusion equation (2.7) for N_1^{ss} for a circular

island of size s centered in a circular CZ of area A with $N_1^{ss} = 0$ on the island boundary, $r = R_{isl} = (s/\pi)^{1/2}$, and a zero flux boundary condition on the CZ boundary, $r = R_{CZ} = (A/\pi)^{1/2}$, to obtain

$$N_1^{ss} = (\tilde{R}_{CZ})^2 \left\{ \frac{1}{2} \ln\left(\frac{\tilde{r}}{\tilde{R}_{isl}}\right) - \frac{1}{4}\left[\left(\frac{\tilde{r}}{\tilde{R}_{CZ}}\right)^2 - \left(\frac{\tilde{R}_{isl}}{\tilde{R}_{CZ}}\right)^2\right]\right\}. \tag{2.10}$$

Here, we set $\tilde{x} = x/r_c$ with $r_c = (h/F)^{1/2}$. From (2.10), we find that $K_{nuc}(CZ) \sim A^{i+2}$ for $s \ll A$.

In our GBS algorithm, islands are nucleated only along CZ boundaries, where N_1^{ss}, and thus the nucleation rate, is relatively large [33]. The probability for selecting various CZ boundary points is not uniform but varies with the local distance, L, between the CZ boundary and the island edge roughly like L^{2i+3}. This appropriately reflects the variation of N_1^{ss} with L. See [34] for more details. For small i, the nucleation rate is substantial at the beginning of the steady-state regime, as the CZs are much larger than their subsequent values for typical $\theta = \mathrm{O}(1)$. This feature is clearly illustrated in Figure 2.1 and is entirely consistent with the conclusions from the rate equation analysis noted above.

To summarize our GBS algorithm, we specify a total island nucleation rate, $K_{nuc}(tot)$, and total island growth rate, $K_{grow}(tot)$, and implement these processes with the correct rates according to the rules prescribed above. In the transient regime, for small i, we neglect island growth; i.e., we set $K_{grow}(tot) = 0$. The procedure for large i is described in section 4. In the steady-state regime, one has $K_{grow}(tot) = FA_{tot}$, where $A_{tot} = L^2$ is the total system area, and individual islands grow at rates given by F times their CZ areas.

Some additional comments on details of the implementation of nucleation are appropriate. One strategy is to monitor the cumulative nucleation rate $M_{isl}(t) = \int_0^t dt K_{nuc}(tot)$ and introduce a new island whenever M_{isl} increases above any integer value. Thus, nucleation times in the transient regime before overlap of DZs are temporally deterministic, with the first island introduced at t_{nuc}, where $M_{isl}(t_{nuc}) = 1$ and

$$\theta_{nuc} = Ft_{nuc} \sim \exp[\beta E_i/(i+2)](h/F)^{-1/(i+2)} L^{-2/(i+2)} \sim \theta^* (L_{isl}^*/L)^{2/(i+2)}. \tag{2.11}$$

Here, $L_{isl}^* = (N_{isl}^*)^{-1/2}$ is the mean island separation at crossover. Thus, in order to achieve the required inequality, $\theta_{nuc} \ll \theta^*$, one must choose the system size so that $L \gg L_{isl}^*$. It is not generally appreciated that one must satisfy this constraint, which is much more severe than just requiring $L \gg L_{isl} = (N_{isl})^{-1/2}$ for N_{isl} values in the steady-state regime. This is a significant issue for multiscale modeling of film deposition where simulation sizes have tended to be relatively small. Later in the deposition process, the nucleation times become random, since after the collision of DZs, A_{nuc} and $K_{nuc}(tot)$ reflect the randomly chosen positions for island nucleation in the transient regime. One can also randomize the earliest nucleation times by suitably choosing to nucleate with a probability proportional to $K_{nuc}(tot)$, but this does not significantly affect the results from the GBS algorithm.

Above, we have sketched the simplest implementation of GBS. Some further details of this implementation, and several significant refinements, are discussed in Appendix A. Finally, we note that accurate determination of the nucleation rate requires precise determination of the product of c_i and σ_i. This is critical for any

multiscale modeling effort but has received little attention. We provide a detailed analysis of σ_i in section 3 and of c_i for canonical models with small i in section 4.

3. Analysis of the capture number σ_i for critical clusters. Here, we present a detailed analysis of the capture number, σ_i, for critical clusters, which significantly extends previous discussions of this important quantity. Below, we adopt the Walton relation for the density of critical clusters, $N_i \approx c_i \exp[-\beta E_i](N_1)^i$, which is discussed further in section 4.

Much of our analysis of capture will exploit the theory of two-dimensional random walks (RWs) on lattices (Polya walks) and is motivated by the work of Tang [38]. We both simplify Tang's analysis for $i = 1$ and extend it to treat $i > 1$. A key RW result that we exploit is that the number of distinct sites visited by a walker after m hops on a square lattice, $S(m)$, satisfies [39]

$$\langle S(m)\rangle \approx \frac{\pi m}{\ln[cm]}, \quad \text{for} \quad m \gg 1, \tag{3.1}$$

where $\langle\ \rangle$ denotes the average over walks. Choosing c slightly below 8 best fits numerical data. Consider a surface populated by a random distribution of "trap sites" of density ρ. The survival probability, $\phi(m)$, that the walker avoids trapping after m hops, and the corresponding trapping probability, $P(m) = 1 - \phi(m)$, satisfy

$$\phi(m) = \langle (1-\rho)^{S(m)}\rangle \approx (1-\rho)^{\langle S(m)\rangle}, \tag{3.2}$$

$$\text{so} \quad P(m) \approx \rho\langle S(m)\rangle \quad \text{for} \quad P(m) \ll 1 \quad \text{and} \quad m \gg 1. \tag{3.3}$$

The approximation in (3.2) for $\phi(m)$ was introduced by Rosenstock [40] and actually constitutes a lower bound on the exact $\phi(m)$ [39].

3.1. Irreversible island formation ($i = 1$). First, we analyze behavior in the early transient regime, where $N_1 \approx Ft$. For $i = 1$, where $c_1 = 1$, consider the probability that an atom deposited at time τ finds a *preexisting* adatom to nucleate a stable island by the time $t > \tau$. From the reference frame of the target trap atom, the deposited atom appears to be hopping with rate $2h$ per each of the four directions on the square lattice, so the total number of hops in the time interval $t-\tau$ is $m = 8h(t-\tau)$. Thus, the probability of trapping is $N_1(\tau)\langle S[8h(t-\tau)]\rangle$, and the total island density at time t, for $ht \gg 1$, is given by

$$\begin{aligned} N_{isl}(t) &\approx \int_0^t d\tau F N_1(\tau)\langle S[8h(t-\tau)]\rangle \\ &\approx 8\pi F^2 h \int_0^t d\tau \frac{\tau(t-\tau)}{\ln[8ch(t-\tau)]} \approx \frac{4\pi}{\ln[4cht]}\frac{(h/F)^3\theta^3}{3}. \end{aligned} \tag{3.4}$$

The constraint of considering the deposited adatom meeting preexisting adatoms avoids double counting. Behavior for $ht < 1$ is described below for the general case of $i \geq 1$.

In the steady-state regime, the density of adatoms, as well as of critical and stable clusters, change slowly on the lifetime of an adatom, τ_{adatom}, where $N_1 \approx F\tau_{adatom}$. The nucleation rate scales like the probability for a deposited atom to diffuse to a critical cluster (here a single atom) within the lifetime, τ_{adatom}, of that deposited adatom. The total number of hops of the deposited atom in the reference frame of the target adatom is $m = 8h\tau_{adatom}$ Thus, we conclude that (cf. [38])

$$\frac{dN_{isl}}{dt} \approx \frac{1}{2}FN_1\langle S(8h\tau_{adatom})\rangle \approx \frac{4\pi}{\ln[8c(h/F)N_1]}h(N_1)^2. \tag{3.5}$$

The factor of 1/2 avoids double counting. It was not needed in the analysis of the transient regime, as we considered nucleation by the depositing atom meeting preexisting adatoms.

Comparing (3.1) with (2.2) and noting that $N_1 \approx Ft$ early in the transient regime, and comparing (3.2) with the general expression for the nucleation rate, we conclude that

$$\sigma_1 \approx \frac{4\pi}{\ln[k_1(h/F)N_1]}, \tag{3.6}$$

where $k_1 \approx 4c$ ($8c$) in the transient (steady-state) regime.

It is not so important to obtain precise values for k_1 since it appears under the ln, but it is important to accurately determine the numerator. As discussed in more detail in section 3.2, equation (3.6) does not apply in the transient regime for very short times $ht < 1$ or $\theta < (h/F)^{-1}$. A well-known derivation of the form (3.6) for the capture number σ_1 for $i = 1$ in the steady-state regime is given by Bales and Chrzan [8]. This work is based on analysis of steady-state deposition-diffusion equations, whose application for nucleation is less clear than for aggregation with stable clusters. Also, this presentation does not address behavior in the transient regime. We would argue that the RW-based derivation is more appropriate and more versatile.

3.2. Reversible island formation ($i > 1$ with $E_i \neq 0$). Again, we first analyze behavior in the early transient regime, where $N_1 \approx Ft$. For $i > 1$, we develop a natural extension of the analysis for $i = 1$. Consider the probability that an atom deposited at time τ finds a critical cluster of i preexisting adatoms to nucleate a stable island by time $t > \tau$. The total number of hops of the deposited atom is $m = 4h(t-\tau)$. Thus, from the associated probability of capture, $N_i(\tau)\langle S[4h(t-\tau)]\rangle$, one obtains

$$\begin{aligned} N_{isl}(t) &\approx (i+1)\int_0^t d\tau F N_i(\tau)\langle S[4h(t-\tau)]\rangle \\ &\approx 4\pi(i+1)c_i \exp[-\beta E_i]F^{i+1}h\int_0^t d\tau \tau^i (t-\tau)/\ln[4ch(t-\tau)] \\ &\approx \frac{4\pi}{\ln[4(i+1)^{-1}cht]} c_i \exp[-\beta E_i](i+2)^{-1}(h/F)^{i+2}\theta^{i+2}. \end{aligned} \tag{3.7}$$

The expression under the first integral accounts for stabilization of a cluster by hopping of the atom deposited at τ adjacent to a critical cluster of i atoms. The factor of $i+1$ accounts for the possibility that the island is stabilized by the hopping of one of the other i preexisting adatoms.

As an aside, we note that the above analysis does not apply for very short times in the transient regime. However, as for any nonequilibrium process involving adsorption and diffusion, one can develop the hierarchical form of the exact master equations for the evolution of the probabilities of various configurations of sites [41]. It is a straightforward matter to see that for $ht < 1$ or, equivalently, for $\theta < (h/F)^{-1}$, nucleation of stable clusters is dominated by direct deposition of adatoms adjacent to critical clusters (which occurs at a rate scaling like $F\theta^i$), rather than by diffusion-mediated aggregation (which occurs at a rate scaling like $h\theta^{i+1}$).

Next, we consider behavior in the steady-state regime. For $i > 1$, it follows that

$$\frac{dN_{isl}}{dt} \approx F N_i \langle S(4h\tau_{adatom})\rangle \approx \frac{4\pi}{\ln[4c(h/F)N_1]} c_i \exp[-\beta E_i] h (N_1)^{i+1}. \tag{3.8}$$

We regard (3.8) as incorporating a factor of $(i+1)$, as in (3.7), since cluster stabilization can occur by the hopping of the deposited atom on which we are focusing or by the hopping of any of i other atoms. However, there is also a compensating factor of $1/(i+1)$ to avoid overcounting. The latter was avoided in (3.7) by considering nucleation involving a deposited atom and preexisting adatoms.

Comparing (3.7) with (2.2) and noting that $N_1 \approx Ft$ in the transient regime, and comparing (3.8) with the general expression for the nucleation rate, we conclude that

$$\sigma_i \approx \frac{4\pi}{\ln[k_i(h/F)N_1]}, \tag{3.9}$$

with $k_i \approx 4(i+1)^{-1}c$ (4c) in the transient (steady-state) regime.

Again, it is not so important to obtain precise values for k_i since it occurs under the ln, but it is important to accurately determine the numerator. Also, (3.9) does not apply for $\theta < (h/F)^{-1}$.

3.3. Refined treatment for $i > 1$ when $E_i = 0$. In section 4, we shall consider canonical models for small i where $E_i = 0$; i.e., adatoms in unstable clusters of size i or less can hop with the same rate as isolated adatoms, leading to rapid dissociation of such clusters. One can certainly adopt the picture of section 3.2 that nucleation occurs when a diffusing adatom reaches a site adjacent to a critical cluster in order to nucleate a stable island. In fact, this formulation will be shown to be reasonably effective in our detailed analysis in section 4. However, an alternative picture appropriate for the special case where $E_i = 0$ instead regards nucleation as resulting from the simultaneous meeting of a deposited atom with i other diffusing adatoms.

For $i = 2$ with $E_2 = 0$, the deposited adatom must simultaneously meet two other diffusing adatoms within the appropriate time interval in order to nucleate a stable island. In the reference frame of the deposited atom (i.e., selecting the origin of a square lattice to coincide with the current location of the deposited atom), the two other diffusing adatoms must simultaneously reach sites forming a connected cluster with the origin of this two-dimensional lattice. This problem is equivalent to a single random walker reaching one of a suitable set of sites nearby the origin on a four-dimensional hypercubic lattice.[1] Likewise, for general $i > 1$ with $E_i = 0$, nucleation is related to the problem of a single random walker reaching a suitable site nearby the origin of a $2i$-dimensional hypercubic lattice.[1] A Rosenstock-type analysis of the probability of a RW in $2i$ dimensions reaching the trap site in the allotted time naturally leads to consideration of the mean number of distinct sites visited by a walker after m hops on the $2i$-dimensional hypercubic lattice, $\langle S(m)\rangle \sim (1-R)m$, for $i > 1$. Here, R is related to the probability of return to the origin for the RW, and $R \to 0$, as $i \to \infty$ [39, 42].[1]

The main point that we wish to note here is that since nucleation in these models with $i > 1$ and $E_i = 0$ corresponds to the trapping of a RW in a dimension above 2, one should not expect any ln factor to appear in the capture number σ_i. This is a direct consequence of the absence of a ln factor in $\langle S(m)\rangle$. Thus, one should regard σ_i as a constant for $i > 1$ and $E_i = 0$.

4. Analysis of canonical models for small critical size ($i = 1, 2, 3$). In this section, we analyze canonical models for $i = 1$, 2, and 3 on a square lattice with

[1] These many-particle diffusion problems in two dimensions do not reduce to a standard RW in higher dimension. Thus, the escape probability will be modified, but basic RW behavior applies.

$E_i = 0$. The choice $E_i = 0$ maximizes the degree of difficulty in nucleating stable clusters (i.e., the degree of reversibility) for $i > 1$. However, we do not expect the resulting behavior to be much different from that for "small" E_i. Specifically, in our atomistic simulation models, adatoms in *unstable clusters* of size i or less can hop at the same rate, h, as isolated adatoms; i.e., there is no stabilization of such clusters. (One minor variant of our model for $i = 3$ has doubly coordinated adatoms in unstable clusters of size 3 also immobile.) Thus, to nucleate a *stable cluster* essentially $i + 1$ diffusing adatoms must simultaneously meet and form a connected cluster (or an atom must be deposited next to a critical cluster). Once such a stable cluster is formed, adatoms within it can never detach. In our atomistic models for $i = 1$, 2, and 3, for adatoms in stable clusters of size $i + 1$ or above, we incorporate edge diffusion of singly coordinated adatoms also at rate h (with both first and second nearest-neighbor hops). This feature allows stable clusters to achieve compact near-square shapes. Doubly coordinated adatoms are immobile. The canonical models and the variant for $i = 3$ are particularly appealing from the perspective of fundamental mathematical analysis and modeling, since behavior depends on a single "control" parameter h/F.

Accurate specification of the nucleation rate is essential for any reliable multiscale modeling. However, as noted above, little analysis exists of the capture number for critical clusters, σ_i, or of the prefactor, c_i, in the Walton relation, both of which affect this rate. In section 3.2, we provided an analysis of the σ_i within a picture where the diffusing adatom must reach a critical cluster to nucleate a stable island. In section 4.1, we provide a corresponding analysis of the c_i for our canonical models. We note again the caveat of section 3.3 that one should select a suitable constant σ_i for these models when $i > 1$, rather than applying (3.9).

4.1. Analysis of coefficient c_i in the Walton relation. Traditionally, c_i corresponds to the number of distinct configurations of the critical cluster with the lowest energy (E_i). This view extends to our canonical models with $E_i = 0$ and unrestricted hopping (at rate h) of adatoms in unstable clusters. This can be demonstrated by a kinetic equation based analysis, as discussed in more detail below. However, the most significant issue is appropriate counting of configurations of critical clusters in our model. For $i = 1$, as always one has $c_1 = 1$. For $i = 2$, normally one just counts horizontal and vertical dimers on neighboring sites (which can be stabilized by the addition of a diffusing atom), yielding $c_2 = 2$. However, in our model, a stable trimer can also be formed by a diffusing atom reaching either of two configurations with 2nd neighbor atoms, or two with 3rd neighbor atoms (see Figure 4.1(a)), so one concludes that $c_2 = 6$. For $i = 3$, normally one just counts two linear and four bent trimers (which can be stabilized by a diffusing atom), yielding $c_3 = 6$. However, in our model, a stable tetramer can also be formed by a diffusing atom reaching the additional 16 configurations shown in Figure 4.1(b). Thus, one has that $c_3 = 22$. Use of these larger values for c_i will be necessary for GBS (or any other multiscale modeling) to produce behavior comparable to that seen in atomistic simulation of our models with $i > 1$ and $E_i = 0$.

Next, we turn to a mean-field analysis for the population of critical clusters based on kinetic equations. For $i > 1$, consider the rate equation for the population of horizontal dimers, N_{2h}. Such a dimer on a specific adjacent pair of sites can be created in six ways by one of those sites being already occupied and another atom hopping onto the second. Given that the population of any configuration of separated adatom pairs roughly equals $(N_1)^2$, for $N_1 \ll 1$, the total gain term in the N_{2h}-

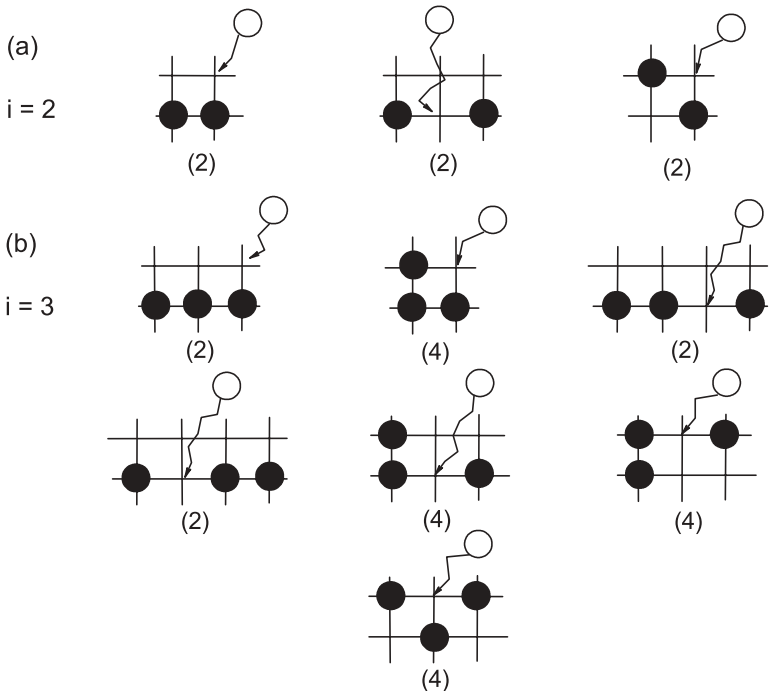

FIG. 4.1. *Approach of an adatom (open circle) to and stabilization of critical clusters (filled circles) in the canonical model on a square lattice with $E_i = 0$ for* (a) $i = 2$; (b) $i = 3$. *Also shown in parentheses is the number of distinct orientations for each of these configurations.*

equation is $6h(N_1)^2$. The loss term in the N_{2h}-equation, $6hN_{2h}$, reflects the six ways that such a dimer can be destroyed by one of its atoms detaching at rate h. See Figure 4.2(a). Thus, making the usual quasi-equilibrium steady-state assumption regarding the population of substable clusters, one has

$$\frac{dN_{2h}}{dt} \approx 6h(N_1)^2 - 6hN_{2h} \approx 0, \quad \text{so} \quad N_{2h} \approx (N_1)^2. \tag{4.1}$$

Similar analysis yields a population of $N_{2v} \approx (N_1)^2$ for vertical dimers, and the same result for each of the horizontal or vertical pairs of 2nd neighbor atoms, and for each of the two orientations of 3rd neighbor pairs of adatoms. Thus, for $i = 2$, one has $N_i \approx 6(N_1)^2$, consistent with the above claim that $c_2 = 6$.

For $i > 2$, consider the rate equation for the population of bent trimers, N_{3b}, say. Such a trimer can be created in three ways by an adatom hopping adjacent to a horizontal dimer of neighboring atoms already on two of those sites and in another three ways by an adatom hopping next to such a vertical dimer of neighboring adatoms. It can also be created in two ways by an adatom hopping into a 2nd neighbor pair of atoms on two of those sites, which has population $(N_1)^2$. Thus, the gain term in the N_{3b}-equation is $3hN_1N_{2h} + 3hN_1N_{2v} + 2h(N_1)^3$. The loss term in the N_{3b}-equation, $m_{3b}hN_{3b}$, reflects the m_{3b} ways that such a trimer can be destroyed by one of its atoms detaching at rate h. See Figure 4.2(b). Making the usual quasi-equilibrium

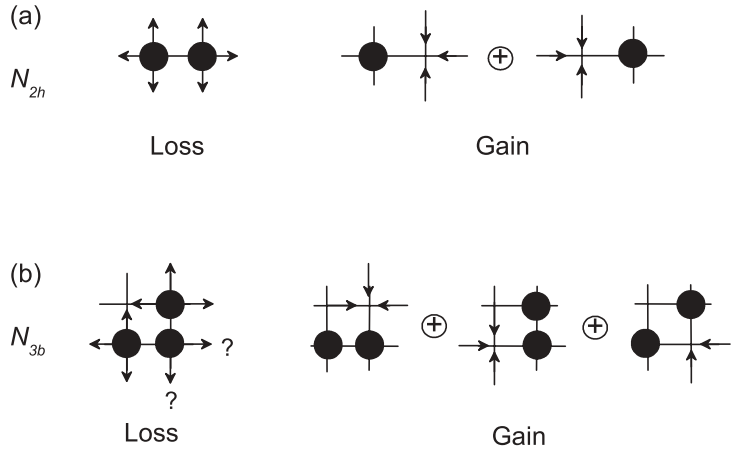

FIG. 4.2. *Dynamic processes associated with loss and gain terms in the kinetic equations for the populations of substable clusters. Examples are shown for* (a) *a horizontal dimer;* (b) *a bent trimer. For the loss term in the latter, the two detachment processes for the middle adatom are allowed in the canonical model but forbidden in its variant.*

steady-state assumption regarding the population of substable clusters, one has

(4.2)
$$\frac{dN_{3b}}{dt} \approx 3hN_1N_{2h} + 3hN_1N_{2v} + 2h(N_1)^3 - m_{3b}hN_{3b} \approx 0, \quad \text{so} \quad N_{3b} \approx \frac{8}{m_{3b}}(N_1)^2.$$

For the canonical model with no restrictions on hopping of adatoms in substable clusters, one has $m_{3b} = 8$, so $N_{3b} \approx (N_1)^3$. However, for the variant of this model where doubly coordinated adatoms are immobile, one has $m_{3b} = 6$ corresponding to a reduction in the destruction rate of bent trimers, so $N_{3b} \approx (4/3)(N_1)^3$ is elevated relative to the canonical model. Complete analysis for $i = 3$ for the canonical model reveals that each of the 22 critical cluster configurations have population roughly equal to $(N_1)^3$, so $N_i = N_3 = 22(N_1)^3$, and $c_3 = 22$, as claimed above. For the variant of this model when $i = 3$, the overall populations are higher, slightly increasing the effective value of c_3 to 23.4. However, the mean-field analysis may not yield a precise value for this variant (see below), since restricting detachment from unstable islands could induce subtle spatial correlations.

Given the significance of appropriate specification of c_i for multiscale modeling, and given the lack of previous detailed consideration, it is appropriate to test the above ideas for other models. Thus, in Appendix B, we present an analysis of nucleation for a variant of a "point-island" model, where it is clear that one should have $c_i = 1$ for all i.

4.2. GBS results. First, in Figure 4.3, we provide a visual comparison of island distributions generated by conventional KMC simulation of our canonical models for $i = 1$, 2, and 3, with results from corresponding GBS studies.

Next, we provide a detailed analysis of the initial behavior of the nucleation rate, K_{nuc}, based on KMC studies of our canonical models in the transient regime for comparison with the theoretical predictions of section 3 and section 4.1. Figure 4.4(a) shows good agreement between KMC results for $i = 1$, and those obtained by GBS for $i = 1$, where $c_1 = 1$, and using (3.6) for σ_1. This agreement should be anticipated from a previous study [8], which demonstrated agreement between KMC and analytic

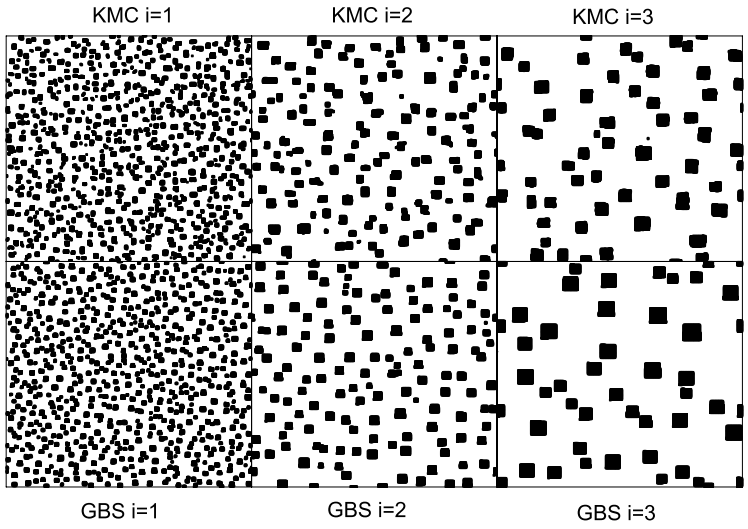

FIG. 4.3. *Comparison of islands distributions from KMC and GBS for our atomistic models with $i = 1$, 2, and 3 and $E_i = 0$. We choose $\theta = 0.1$ ML, $h/F = 10^6$, and the variant model for $i = 3$. The images show a region of 500×500 lattice sites.*

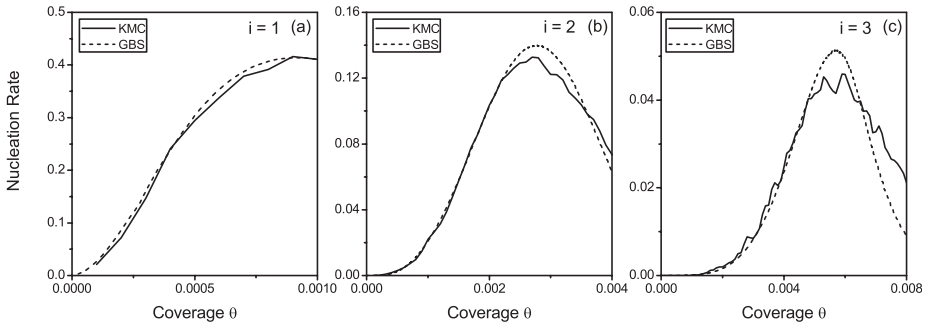

FIG. 4.4. *Comparison of the initial behavior of the nucleation rates for GBS and KMC simulations of our atomistic models with $i = 1$, 2, and 3 and $E_i = 0$. We choose $h/F = 10^6$ and the variant model for $i = 3$.*

results using (3.6) for σ_1. For $i = 2$, good agreement of KMC and GBS results for K_{nuc} is shown in Figure 4.4(b) choosing $c_2\sigma_2 \approx 16$. This is consistent with our proposed value of $c_2 = 6$ and a choice of $\sigma_2 = 2.6$ slightly above typical values based on (3.9). In contrast, a large discrepancy arises using the traditional value of $c_2 = 2$ and any $\sigma_2 \approx 2 - 3$. For $i = 3$, agreement of KMC and GBS results for K_{nuc} shown in Figure 4.4(c) for the variant of the canonical model (where doubly coordinated adatoms in the middle of a trimer cannot hop) requires a choice of $c_3\sigma_3 \approx 100$. Given our analysis of $c_3 \approx 25$ in section 4.1, this result implies a value of $\sigma_3 \approx 4$. This is significantly above typical values for capture number based on (3.9), a feature which perhaps reflects the special nature of capture associated with $E_i = 0$ as discussed in section 3.3. Of course, using the traditional value of $c_3 = 6$ would imply an unreasonably large value for σ_3 of roughly 16–17.

As an aside, for $i = 3$, we have also examined the initial behavior of K_{nuc} for

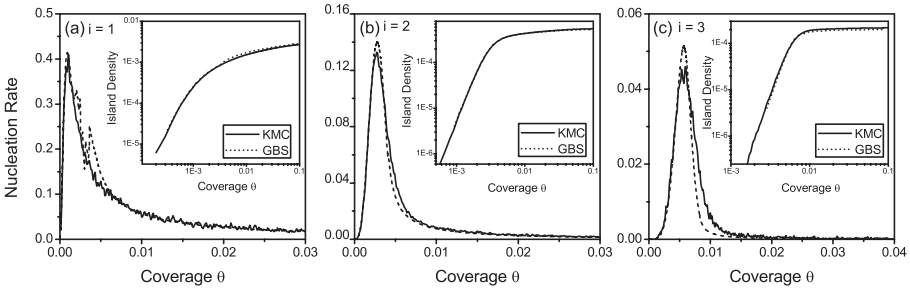

FIG. 4.5. *Comparison of the overall behavior of the nucleation rates, as well as predictions for the mean island density, N_{isl} versus θ, for GBS and KMC simulations of our atomistic models with $i = 1$, 2, and 3 and $E_i = 0$. We choose $h/F = 10^6$ and the variant model for $i = 3$.*

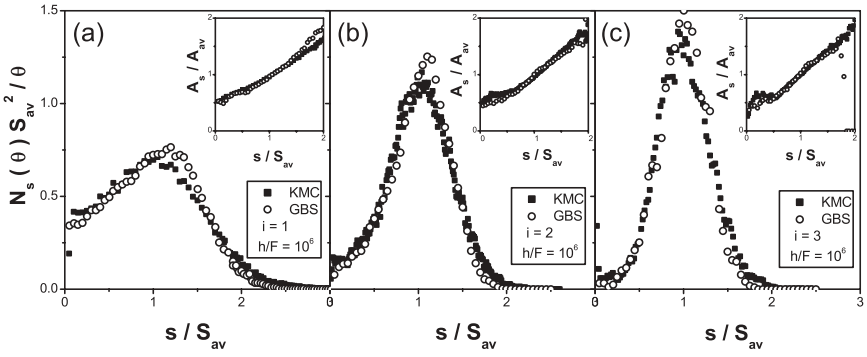

FIG. 4.6. *Comparison of the scaled island size distribution for GBS and KMC simulations of our atomistic models with $i = 1$, 2, and 3 and $E_i = 0$. We choose $\theta = 0.1$ ML, $h/F = 10^6$, and the variant model for $i = 3$. Here N_s is the density per site of islands of s adatoms. The insets show the behavior of the mean CZ area (for islands of a specific size, s) versus island size. The increase with s is much faster than mean-field predictions.*

the canonical model where all adatoms in substable trimers can hop with rate h (in contrast to the variant described above). We find that $c_3\sigma_3$ is a somewhat smaller value for the canonical model than the variant (by a factor of roughly 0.89). This is consistent with our analysis in section 4.1, indicating that c_3, and thus the density of critical clusters, is lower (by a factor of 0.94).

Extending the above analysis of initial nucleation, in Figure 4.5, we compare the nucleation rate and mean island density obtained from KMC studies over a broader range of coverage up to 0.1 ML with corresponding results from GBS. For the latter, note that we switch between distinct transient regime and steady-state regime algorithms for determining these quantities when $\theta \approx \theta^*$. Again, the agreement is shown to be excellent, supporting the validity of the GBS approach.

Finally, we emphasize that GBS can reliably obtain much more detailed information on the island distribution, including the island size distribution, the CZ area distribution, and even the joint probability distribution for these quantities [33, 34]. This is significant since conventional mean-field rate equation treatments fail qualitatively to predict the correct behavior of these quantities [5, 9]. In Figure 4.6, we compare KMC and GBS results for i =1–3 for the island size distribution and for the average CZ area (for a specific island size) versus island size for $h/F = 10^6$ at fixed $\theta = 0.1$ ML. Again, agreement is excellent.

5. Analysis of behavior for large critical size ($i = 6, 15$). We recall that a primary motivation for developing multiscale methods to study island formation during deposition was to explore the regime of highly reversible island formation (large i) where conventional KMC of atomistic models is inefficient. To fulfill this goal, we first present results for critical size significantly larger than the standard choices of $i = 1$, 2, or 3 examined in KMC studies.

5.1. DZ and island growth in the transient regime. A significant difference between behavior for large critical size that for $i = 1$, 2, or 3 is that the transient regime is expanded and that both island nucleation and growth become more significant in this regime. In particular, island growth in the transient regime for large i should not be neglected as done above for $i = 1$, 2, and 3. A straightforward geometry-based picture of island growth in this regime starts with the observation that the DZ radius grows like $R_{DZ}(\delta t) \sim (h\delta t)^{1/2}$, where δt is the time since nucleation [34]. It then follows that the subsequent island size, $S_{av}(\delta t)$, is given by the cumulative number of atoms deposited within the growing DZ. Thus, prior to DZ collision and coalescence, S_{av} satisfies

$$S_{av}(\delta t) \approx F \int_0^{\delta t} du \pi R_{DZ}(u)^2 \approx \frac{1}{2}(h/F)(\delta\theta)^2, \tag{5.1}$$

where $\delta\theta = F\delta t$ is the increase in coverage since nucleation. Choosing $\delta\theta \sim \theta^* = F\delta t^*$, it immediately follows that $S_{av}(\delta t^*) \sim S^*_{av}$, consistent with the analysis in section 2.1. Thus, the simplest refinement of the basic GBS algorithm to incorporate island growth in the transient regime simply tracks the nucleation times, t_{nuc}, or coverages, $\theta_{nuc} = Ft_{nuc}$, of various islands, and then assigns sizes, $S_{av}(t^* - t_{nuc})$, at θ^* based on the above formula. An understanding of the island size distribution at θ^* is also possible. It comes from the recognition that the population, N^*_s, of islands of a certain size, s, is proportional to the nucleation rate at that prior time which would produce islands of size s at θ^*. See Appendix C.

Previous precise treatment of DZ growth for small i solved the appropriate time-dependent deposition-diffusion equation (2.7) for DZ expansion about a "point island" with fixed size. However, for large i, significant growth of the island during the transient regime is expected to impact (and enhance) growth of the DZ. Thus, here we show how to incorporate the influence of island growth into analysis of (2.7) for $t > t_{nuc}$, in the range $r > R_{isl}(t)$, where $R_{isl}(t)$ is the growing radius of an isolated circular island. Here, we impose the boundary condition $N_1(r = R_{isl}, t) = 0$, and also set the initial condition that $N_1(r, t = t_{nuc}) = \theta_{nuc}$, for $r > R_{isl}$.

One could attempt to self-consistently solve this moving boundary value problem, where the island radius is determined from suitably integrating the diffusive flux at R_{isl}, which is in turn determined from solution of (2.7). However, we will adopt the simpler but reasonable approach of incorporating an approximate form of R_{isl} from (5.1) as $R_{isl}(t) = [S_{av}(\delta t)/\pi]^{1/2}$. One can then transform the above boundary value problem into one with a fixed boundary in terms of the new variable $\delta r = r - R_{isl}(t) \geq 0$. To recast this equation in the most natural dimensionless form, one also replaces the variable t by θ and rescales the radial distance as $\delta\tilde{r} = \delta r/r_c \geq 0$ with $r_c = (h/F)^{1/2}$. Then, *neglecting the nucleation term*, (2.7) becomes

$$\frac{\partial N_1}{\partial \theta} = 1 + \left[\frac{\partial^2}{\partial(\delta\tilde{r})^2} + \frac{1}{\delta\tilde{r} + \theta/\sqrt{2}}\frac{\partial}{\partial(\delta\tilde{r})}\right] N_1 + \frac{1}{\sqrt{2}}\frac{\partial N_1}{\partial(\delta\tilde{r})}, \quad \text{for} \quad \theta > \theta_{nuc}, \tag{5.2}$$

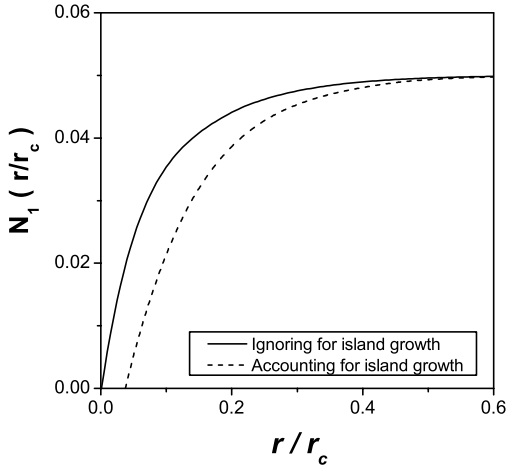

FIG. 5.1. *N_1 versus r for $\theta_{nuc} = 0$ and $\theta = \theta^*$ obtained from solution of the time-dependent deposition-diffusion equations. Comparison of behavior ignoring and accounting for island growth.*

in the range $\tilde{r} \geq 0$ with boundary condition $N_1(\delta\tilde{r} = 0, \theta) = 0$ and initial condition $N_1(\delta\tilde{r}, \theta_{nuc}) = \theta_{nuc}$.

We define R_{DZ} so that nucleation outside the DZ at a uniform rate based on the approximation $N_1 \approx \theta$ will recover the exact nucleation rate

$$\int_{R_{isl}}^{R^+} 2\pi r dr N_1(r,t)^{i+1} = \int_{R_{DZ}(t)}^{R^+} 2\pi r dr (\theta \approx Ft)^{i+1}, \tag{5.3}$$

where R^+ is a suitable upper cut-off [33, 34]. From the above prescription, it is clear that $R_{DZ} > R_{isl}$ for $t > t_{nuc}$ will increase from its initial value of R_{isl} at $t = t_{nuc}$. In Figure 5.1, we compare behavior based on the above treatment with the simpler formulation neglecting island growth.

5.2. Parameter selection and GBS results for large *i*. In comparing behavior for different large i (and some specific θ), it is appropriate to choose model parameters in some systematic fashion. To this end, we choose the two key parameters, h/F and E_i, by imposing two constraints: fix both island density to $\sim 10^{-4}$ per site at ~ 0.1 ML and fix $\theta^* \approx 0.05$ ML. Using the scaling results of section 2.1, one has that

$$\theta^* \sim \exp[\beta E_i/i] \quad \text{and} \quad N_{isl} \sim \exp[-\beta E_i/i](h/F)^{-1} \quad \text{for large } i. \tag{5.4}$$

Thus, the above constraints imply that $\beta E_i/i \to -3.0$ and $h/F \to 10^{5.3}$, as $i \to \infty$. In this section, we will consider just $i = 6$, and $i = 15$. For $i = 6$, one has $\beta E_6 \approx -1.8$ and $h/F \approx 10^{5.5}$. For $i = 15$, one has $\beta E_{15} \approx -29$ and $h/F \approx 10^{5.4}$.

The case $i = 6$ corresponds to the regime of stable septamers for deposition on an fcc(111). In such systems, one expects transitions with increasing temperature from $i = 1$ (stable dimers with no bond breaking) to $i = 2$ (stable tetramers with single but not double bond breaking) to $i = 6$ (stable septamers with single and double but not triple bond breaking). In the latter regime, the critical cluster consists of the septamer but is missing one of the six peripheral atoms, so $c_6 = 6$. The case $i = 15$ might correspond to, e.g., stable 4×4 clusters on a square lattice, where the

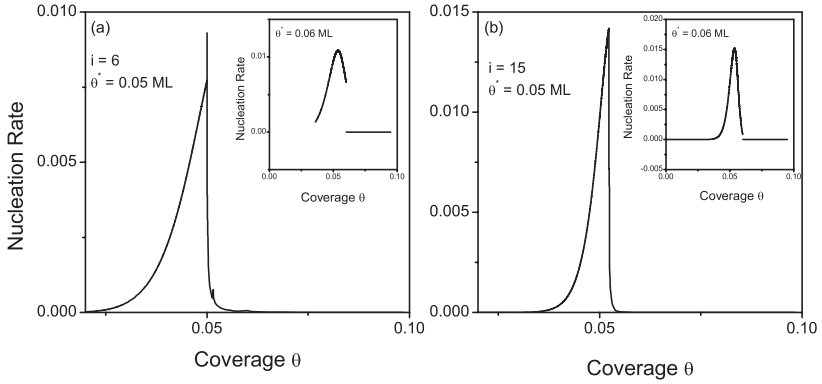

FIG. 5.2. *Nucleation rates versus coverage for critical sizes, $i = 6$ and 15, for models with parameters chosen as described in the text. Also indicated in the insets is the dependence on the choice of coverage where we switch from the transient to the steady-state GBS algorithm.*

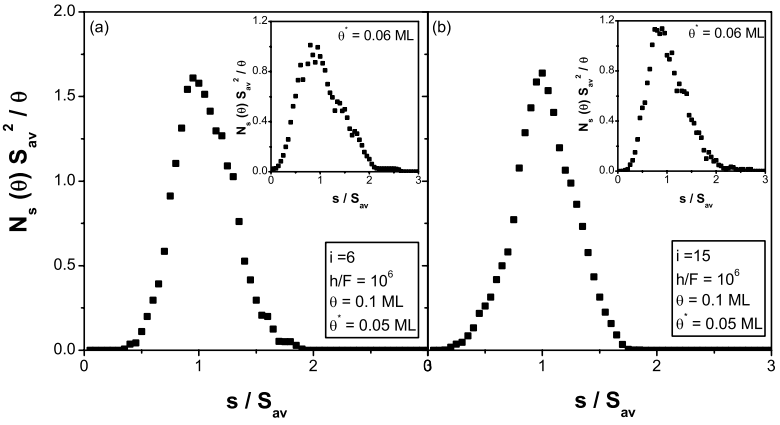

FIG. 5.3. *Island size distributions for critical sizes, $i = 6$ and 15, for models with parameters chosen as described in the text. Also shown in the insets is behavior for a poorer choice of coverage where we switch from the transient to the steady-state GBS algorithm.*

critical cluster is a 4×4 cluster with one of the four corner atoms missing, so $c_4 = 4$. However, $i = 15$ is a somewhat artificial example, as there is no reason why 4×4 clusters should be significantly more stable than 3×3 or 2×2 clusters.

Figure 5.2 shows the behavior of the nucleation rate for these i in the GBS formulation. Results demonstrate the need to choose an appropriate coverage to switch from transient to steady-state algorithms. Figure 5.3 shows corresponding results for the island size distributions. There have been no KMC studies or previous studies by other multiscale methods of these size distributions for large i. The trend of sharpening the island size distribution for increasing small i up to ~ 6 does not persist for large i. Indeed, the factors controlling the shape of this distribution are subtle. Increasing i above unity delays the onset of nucleation, while still preserving most nucleation along CZ boundaries in the steady-state regime. This helps to sharpen the distribution. However, for large i, a significant fraction of nucleation occurs in the transient regime and around crossover, where nucleation positions are more random. This seems to offset the trend towards sharpening. We should caution that the GBS

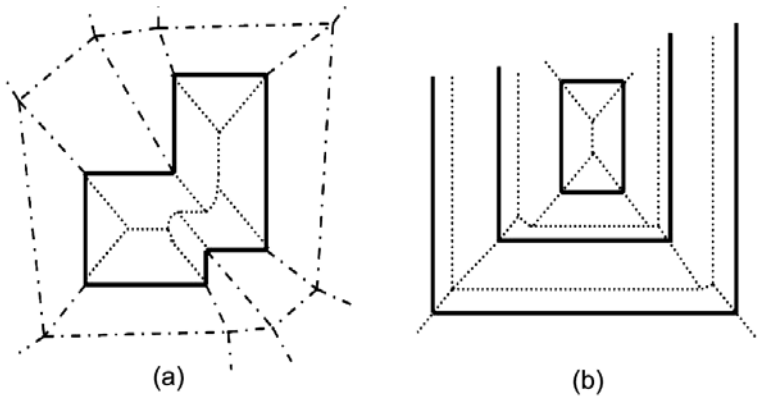

FIG. 6.1. (a) *Schematic of sub-CZs for a pair of coalesced islands in the submonolayer regime.* (b) *Schematic of sub-CZs for a multilayer stack of three islands. CZ boundary positions between ascending and descending step edges reflect the presence of a step-edge barrier. Nucleation is implemented along "internal" sub-CZ boundaries which are not connected directly to step edges.*

results presented here do not include a separate and precise treatment of the crossover regime, so this may limit the precision of our results for the size distribution.

6. Extension of GBS to treat island coalescence and multilayer growth. In order to develop a GBS-based treatment of multilayer growth, it is necessary to first prescribe a treatment of island coalescence in the submonolayer regime for coverages above ~ 0.3 ML. Hence, this is done first in section 6.1. Then, in section 6.2, we provide some comments on the key components of a treatment of multilayer growth focusing on the case of significant step-edge barriers.

6.1. Island coalescence regime. In the treatment above of the precoalescence regime, our GBS algorithm simply prescribes near-square shapes for individual islands. This is quite appropriate and realistic for metal(100) homoepitaxy [37]. However, to extend GBS to the regimes of island coalescence and percolation at higher submonolayer coverages, one must have an appropriate prescription for growth coalescence shapes. A recent simulation study and theoretical development for growth coalescence shapes in metal(100) systems indicates preference for maintenance of "geometric" shapes with straight edges aligned with principal lattice directions (as are sides of individual square islands prior to coalescence) [32]. Given the propensity for straight edges, it is natural to track growth into the coalescence regime by exploiting the concept of sub-CZs for each edge segment [10, 11]. See Figure 6.1. The idea is simply that the complete CZ for each island or coalesced cluster of islands can be decomposed into sub-CZs for each island edge segment such that the rate of attachment to that edge segment is in exact proportion to the sub-CZ area. These sub-CZs could be determined exactly from analysis of the appropriate deposition-diffusion equation, but for GBS, one expects that it will suffice to implement a simpler Voronoi-type construction. Once the sub-CZs are constructed, the growth velocity of each straight edge segment is readily determined (neglecting significant mass transport between edge segments), and thus step-edge evolution can be implemented within the GBS formulation.

6.2. Multilayer growth regime. In the simplest case of layer-by-layer growth, one would simply repeat the GBS procedure after each monolayer deposition; i.e.,

there would first be a transient regime where the adatom population increases, followed by a steady-state regime. To avoid the complication of repeatedly switching between transient and steady-state regimes, henceforth we consider only the case of a significant additional Ehrlich–Schwoebel (ES) step-edge barrier, E_{ES}, inhibiting downward transport [35, 36]. Specifically, this barrier should be sufficiently strong that there is significant second-layer island nucleation before completion of 1 ML deposition. This implies that after the brief transient regime at the onset of submonolayer deposition, a steady-state regime will always apply. For the latter, the adatom density is controlled by a balance between gain due to deposition, and loss due to aggregation, with island steps in the same layer and with descending steps.

The first step in a GBS treatment is the construction of suitable CZs (and sub-CZs) for the multilayer morphologies, followed by appropriate specification of island nucleation (primarily in the highest layers at near the tops of multilayer stacks of islands or "mounds") and island growth. As for submonolayer growth, exact construction of CZs follows from the solution of the appropriate boundary value problem for the steady-state deposition-diffusion equation. For submonolayer growth, the boundary condition at the (ascending) steps of island is simply that the adatom density vanishes, i.e., $N_1 = 0$. For multilayer growth (and also submonolayer growth in the island coalescence regime), one must also impose the appropriate boundary condition at descending steps which reflects the presence of a step-edge barrier. This condition has the form [43]

$$a \left| n.\frac{dN_1}{dr} \right| = \frac{N_1}{L_{ES}}, \tag{6.1}$$

where n is the unit normal vector to the step edge, and a is surface lattice constant. Here, $L_{ES} = \exp[\beta E_{ES}] - 1$ is the ES length, where $L_{ES} = 0$ for $E_{ES} = 0$, and $L_{ES} = \infty$ for $E_{ES} = \infty$, so this boundary condition simply reduces to $N_1 = 0$ for $E_{ES} = 0$. (As in the treatment of submonolayer growth, we neglect the background equilibrium density of adatoms, as this is dominated by the supersaturation density due to deposition.) The most significant effect of this boundary condition will be seen for terraces between an ascending and descending step, where the CZ boundary will be shifted from roughly midway between the steps for $E_{ES} = 0$ towards the descending step for $E_{ES} > 0$. This is simply because the ES barrier inhibits capture at the descending step. For protracted multilayer growth, one expects that typically the length of such terraces is much greater than their width, L. Then, analysis of the corresponding one-dimensional boundary value problem reveals that the ratio of the distances between the CZ boundary and the ascending and descending steps is given by $1 + 2(L_{ES}/L)$.

For an efficient but approximate construction of CZs in multilayer morphologies, one could apply the above rule to determine CZ boundaries between all ascending and descending steps. See Figure 6.1(b). For sub-CZs on "top" terraces surrounded by descending steps (e.g., Figure 6.1(a)), the precise position of the sub-CZ boundaries will be affected by the presence of the step-edge barrier. However, we expect that a simpler Voronoi construction based on the distance to step edges will provide a reasonable approximation. Once the sub-CZs are constructed, all island edge segments are advanced at velocities determined by the associated sub-CZ areas (just as in section 6.1).

The more complicated aspect of GBS is the appropriate implementation of nucleation of new islands. By analogy with our treatment of submonolayer deposition,

nucleation positions are chosen along those "internal" sub-CZ boundary segments which are not connected to step edges and where the local adatom density is expected to be relatively high. Such segments occur between ascending and descending steps (see Figure 6.1(b)), as well as on top terraces surrounded by descending steps (see Figure 6.1(a)). As for submonolayer growth, one must estimate the steady-state adatom density in order to estimate the nucleation rate along different internal sub-CZ boundaries. This is more difficult than in the case of submonolayer CZs, but at least crude estimates could be developed based on one-dimensional approximations to the geometry. Then, the local nucleation rate will reflect the magnitude of the local adatom density. The highest nucleation rates will typically be on top terraces, where the adatom density is highest due to the step-edge barrier. As noted above, the discussion here is based on the presence of a significant step-edge barrier. However, we note that if this barrier is very high, then adatom density on top terraces will become spatially uniform, and then nucleation positions should also be chosen more randomly on such terraces, rather than along internal sub-CZ boundaries.

7. Extension of GBS to treat other nucleation mechanisms.

7.1. Nucleation with desorption (incomplete condensation). In this case, homogeneous nucleation occurs as previously, but now adatoms can also desorb from the surface at rate d per unit time [4, 44]. Desorption introduces a new characteristic length, $L_d = (h\tau_d)^{1/2}$, where $\tau_d = 1/d$ is the lifetime of adatoms (prior to desorption). The dependence of the mean island separation on d s indicated by $L_{isl} = L_{isl}(d)$. If $L_d \gg L_{isl}(d=0)$, where the latter is the mean island separation in the absence of desorption, then adatoms can typically find islands before desorbing, and one observes behavior similar to that for $d = 0$. If $L_d < L_{isl}(d=0)$, then desorption significantly modifies behavior.

For $L_d < L_{isl}(d=0)$, DZs will initially expand with $R_{DZ} \sim (h\delta t)^{1/2}$, as for $d = 0$, but then they will saturate when R_{DZ} reaches $\sim L_d$ (or, more precisely, when $R_{DZ} - R_{isl}$ reaches $\sim L_d$). Thereafter, DZ growth is slaved to island growth such that $R_{DZ}(t) \sim R_{isl}(t) + L_d$. This picture follows from analysis of the time-dependent deposition-desorption-diffusion equation

$$\frac{dN_1}{dt} = F - (i+1)K_{nuc} - dN_1 + h\nabla^2 N_1 = F - (i+1)K_{nuc} - dN_1 + h\frac{1}{r}\frac{\partial}{\partial r}\left(r\frac{\partial}{\partial r}\right)N_1, \tag{7.1}$$

with boundary condition $N_1 = 0$ at $r = R_{isl}$, and where $K_{nuc} = c_i\sigma_i h\exp[-\beta E_i](N_1)^{i+1}$ as before. Neglecting this nucleation term, which will be less significant than for $d = 0$, the quasi-stationary slaved solution has the form

$$N_1 \approx \frac{F}{d}\left[1 - \frac{K_0(r/L_d)}{K_0(R_{isl}/L_d)}\right]. \tag{7.2}$$

In this regime, a GBS approach would maintain homogeneous nucleation in the region outside the DZs at a rate $K_{nuc} = \sigma_i c_i h\exp[-\beta E_i](\theta_-)^{i+1}$ per site, where $N_1 = \theta_-$ satisfies $dN_1/dt = F - (i+1)K_{nuc} - dN_1$. For large d or small L_d, the DZs are narrow rings surrounding islands. The islands grow at constant velocity, and nucleation continues to occur randomly over most of the surface. This is just the standard Avrami model for nucleation and growth [45].

In the GBS formulation, initially, one would nucleate islands at random outside DZs at the rate specified above. When the DZs have expanded to cover most of the

surface, one would tessellate the surface into CZs surrounding each island. Then, the integrated nucleation rate for each CZ is estimated from the solution of the steady-state version of the deposition-diffusion equation (7.1) for N_1^{ss} for a circular island of size s centered in a circular CZ of area A with $N_1^{ss} = 0$ on the island boundary, $r = R_{isl} = (s/\pi)^{1/2}$, and a zero flux boundary condition on the CZ boundary, $r = R_{CZ} = (A/\pi)^{1/2}$. This solution is readily obtained as the sum of the constant particular solution, F/d, and a suitable linear combination of the homogeneous solutions which are Bessel functions $I_0(r/L_d)$ and $K_0(r/L_d)$. Finally, the total nucleation rate is obtained by summing over these rates for individual CZs, as for $d = 0$. Nucleation is implemented preferentially along CZ boundaries.

There are some technical complications relative to the case $d = 0$. First, the crossover from transient to steady-state regimes is more extended, and thus more difficult to treat (cf. item (ii) in Appendix A). Second, the propensity for nucleation along CZ boundaries in the steady-state regime will be less pronounced for $d > 0$ than $d = 0$ since N_1^{ss} will not be so strongly peaked along those boundaries. Nonetheless, we have found that even the simplest GBS treatment obtains crossover from conventional island size distribution for small d to the expected monotonically decreasing Avrami form for large d [46].

7.2. Heterogeneous nucleation pathway. Here, nucleation can occur when diffusing adatoms reach static (defect or impurity) trap sites [47]. When the separation between such trap sites falls below the diffusion length characterizing homogeneous nucleation, it is clear that the heterogeneous nucleation pathway will dominate. In the complete absence of homogeneous nucleation, it is clear that the island size distribution will simply reflect the CZ area distribution generated by a Voronoi-type tessellation of the surface based on the trap sites (at least for the large average CZ area) [48]. This has been confirmed for the case of randomly distributed defects, where the CZ area distribution has the form of a Gamma distribution [49]. Thus, this process is naturally amenable to a GBS-type treatment. One caveat is that for small CZ areas, the island size distribution is more accurately determined by convoluting the CZ area distribution with a Poisson distribution which reflects fluctuations in the number of atoms deposited within each CZ [48]. The GBS approach would not be able to naturally treat such fluctuations.

Perhaps the most interesting or complex behavior is in the crossover regime where competition between homogeneous nucleation at rate $K_{nuc} = \sigma_i c_i h \exp[-\beta E_i](N_1)^{i+1}$ per site and heterogeneous nucleation at rate $K_T = \sigma_T h N_1 \rho_f$ exists. Here, N_1 is the average adatom density, and ρ_f is the density of traps free of adatoms. Also, σ_T denotes the capture number for traps which can be determined from the formalism of section 3, noting that traps here are static. To describe the initial growth of DZs about just-nucleated islands, one uses the time-dependent deposition-diffusion equation

$$\frac{dN_1}{dt} = F - (i+1)K_{nuc} - K_T + h\nabla^2 N_1. \tag{7.3}$$

Homogeneous nucleation outside DZs is implemented at a uniform rate K_{nuc} where $N_1 = \theta_-$ satisfies

$$\frac{dN_1}{dt} = F - (i+1)K_{nuc} - K_T, \quad \text{and} \quad \frac{d\rho_f}{dt} = -\sigma_T h N_1 \rho_f. \tag{7.4}$$

Heterogeneous nucleation outside DZs occurs at each free trap at rate $\sigma_T h \theta_-$. After significant DZ collision, we tessellate the surface into CZs about each island. Ho-

mogeneous nucleation will proceed along CZ boundaries as in the absence of traps, and heterogeneous nucleation at a rate $\sigma_T h N_1^{ss}$ at each free trap, where N_1^{ss} is the steady-state adatom density at the trap determined from the approximation (2.10).

7.3. Exchange-mediated nucleation pathway. Here, nucleation occurs following the exchange of a single adatom with a substrate atom at rate $h_{ex}N_1$, where one usually writes the exchange rate as $h_{ex} = \sigma_0 h$. This nucleation pathway is usually denoted by $i = 0$ [50]. In the absence of conventional homogeneous nucleation, simple mean-field rate equation analysis indicates that the behavior of N_{isl}, and also of the island size distribution, is controlled primarily by the ratio σ_0/σ_{av} [50]. The latter has a monotonically decreasing form [50]. Analysis of spatial aspects of initial behavior, specifically growth of DZs about just-nucleated islands, follows from the time-dependent deposition-diffusion equation

$$\frac{dN_1}{dt} = F - h_{ex}N_1 + h\nabla^2 N_1 = F - h_{ex}N_1 + h\frac{1}{r}\frac{\partial}{\partial r}\left(r\frac{\partial}{\partial r}\right)N_1, \tag{7.5}$$

with boundary condition $N_1 = 0$ at $r = R_{isl}$. DZs initially expand with $R_{DZ} \sim (h\delta t)^{1/2}$ as for $h_{ex} = 0$, but then they will saturate when R_{DZ} reaches $L_{ex} = (\sigma_0)^{-1/2}$ or, more precisely, when $R_{DZ} - R_{isl}$ reaches $\sim L_{ex}$. This quasi-stationary slaved solution has the form (cf. (7.2))

$$N_1 \approx \frac{F}{h_{ex}}\left[1 - \frac{K_0(r/L_{ex})}{K_0(R_{isl}/L_{ex})}\right]. \tag{7.6}$$

In a GBS formulation, initially one would incorporate exchange-mediated nucleation in the region outside the DZs at rate $K_{ex} = h_{ex}(\theta_-)$. Here $N_1 = \theta_-$ satisfies $dN_1/dt = F - h_{ex}N_1$. After significant DZ collision, we tessellate the surface into CZs about each island. Integrated exchange-mediated nucleation rates are determined for each CZ from the steady-state solution, N_1^{ss}, of (7.5) for a circular island in the center of a circular CZ (analogous to the case of nucleation in the presence of desorption). GBS implements nucleation preferentially along CZ boundaries.

7.4. Nucleation with significant dimer mobility. A possible scenario for irreversible island formation ($i = 1$) in metal(100) or metal(111) homoepitaxy is that adsorbed dimers have significant mobility, as described by an effective hop rate h' (i.e., h' is comparable to the adatom hop rate h). Here, we assume trimers and larger clusters are relatively immobile, but it is clear that the method described below can be extended to treat such cases. Then, for comparable h and h', formation of stable immobile islands of three or more adatoms occurs primarily by aggregation of diffusing dimers and adatoms. Consequently, the nucleation rate per site has the form $K'_{nuc} \approx \sigma_2(h + h')N_1N_2$, where N_2 is the density per site of mobile dimers. In this case, the density of stable immobile islands, N_{isl}, has fundamentally different scaling behavior from the case $h' = 0$ [51, 52], and the island size distribution has a different shape [53].

In the early transient regime, $N_1 \approx Ft = \theta$ and $N_2 \approx \sigma_1 h\theta^3/3$ are uniform outside DZs expanding about immobile stable islands of three atoms. Thus, in the GBS formulation, nucleation is also implemented uniformly in this region with the appropriate rate. For $h \approx h'$, DZ growth is similar to $h' = 0$ in the sense that $R_{DZ}(\delta t) \sim (h\delta t)^{1/2}$, but a more precise characterization comes from analysis of the

coupled pair of deposition-diffusion equations

(7.7)
$$\frac{dN_1}{dt} = F - \sigma_1 h (N_1)^2 - K'_{nuc} + h\nabla^2 N_1 = F - \sigma_1 h (N_1)^2 - K'_{nuc} + h\frac{1}{r}\frac{\partial}{\partial r}\left(r\frac{\partial}{\partial r}\right) N_1,$$

(7.8)
$$\frac{dN_2}{dt} = \sigma_1 h (N_1)^2 - K'_{nuc} + h'\nabla^2 N_2 = \sigma_1 h (N_1)^2 - K'_{nuc} + h'\frac{1}{r}\frac{\partial}{\partial r}\left(r\frac{\partial}{\partial r}\right) N_2,$$

with boundary condition $N_1 = N_2 = 0$ at the edge $r = R_{isl}$ of a stable immobile circular island.

After significant DZ collision, we tessellate the surface into CZs about each island and treat this steady-state regime analogously to the case $h' = 0$. Then, the integrated nucleation rate for each CZ is estimated from the solution of the steady-state version of the deposition-diffusion equation (7.7) for N_1^{ss} and (7.8) for N_2^{ss} in a circular geometry approximation, neglecting the K'_{nuc} term. Specifically, we consider a circular island of size s centered in a circular CZ of area A with $N_1^{ss} = 0$ and $N_2^{ss} = 0$ on the island boundary, $r = R_{isl} = (s/\pi)^{1/2}$, and a zero flux boundary condition on the CZ boundary, $r = R_{CZ} = (A/\pi)^{1/2}$. The solution of (7.7) for N_1^{ss} is given by (2.10) since loss due to dimer formation is small. The solution of (7.8) for N_2^{ss} is obtained as the sum of a particular solution, and a suitable linear combination of the homogeneous solutions, which are the constant function and $\ln(r)$. The particular solution for N_2^{ss} is obtained by quadrature, given the form of N_1^{ss} from (7.7). Finally, the total nucleation rate is obtained by summing over the nucleation rates for individual CZs, as for $d = 0$. Nucleation is implemented preferentially along CZ boundaries.

8. Conclusions. We have demonstrated that GBS is an effective approach for precise determination of island densities and distributions during submonolayer deposition. It has been shown to accurately predict behavior for canonical atomistic models for small i but also to effectively treat the regime of large i where conventional KMC simulation is inefficient. The latter has been a central motivation and goal of multiscale treatments of these problems. We have also discussed the versatility of GBS in treating a variety of nucleation mechanisms. However, in addition to its computational capabilities, we should also emphasize the tremendous instructive value of GBS in terms of elucidating the essential features of the island formation process, much like other continuum and hybrid formulations.

Finally, we should note that a still sought-after goal is a reliable fully analytic beyond-mean-field treatment of island formation during deposition [54, 55, 56, 57, 58, 59, 60]. A major challenge in this effort is incorporation into the theory of a realistic treatment of the spatial aspects of nucleation and its impact on evolution of the CZ distribution [59]. It is exactly this feature of the process on which GBS provides considerable insight.

Appendix A. Details and refinements of GBS algorithms.

(i) In the transient regime, accurate evaluation of $K_{nuc}(tot)$ in (2.8) requires determination of A_{nuc}. Prior to the collision of DZs, one has that $A_{nuc} = A_{tot} - \sum_j \pi R_{DZ}^2(j)$, where the sum is over all nucleated islands (labeled by j). The R_{DZ} are determined by analysis of the time-dependent deposition-diffusion equation of a DZ growing about a single island. Subsequent to DZ collision, taking A_{nuc} as the area outside DZs (but still using R_{DZ} from the single island problem) was shown to somewhat overestimate A_{nuc}, and thus to overestimate the nucleation rate [34]. To

correct for the simplest estimate, which we denote by $A_{nuc}(DZ)$, one could use the formula $A_{nuc} = F[A_{nuc}(DZ)]A_{nuc}(DZ)$, where $0 \le F \le 1$. Prior to DZ collision, where $A_{nuc}(DZ) \ge 0.75$, one expects $F \approx 1$. However, after significant collision, we expect that $F < 1$, based on our analysis of DZ growth about a pair of islands, so one might choose, e.g., $F[x] \approx \exp[-c(x-1)^2]$. This correction with $c = 3$ is used only for $i = 3$ in section 4.2.

(ii) In previous studies [33, 34], we introduced a separate treatment of the crossover regime where there is significant overlap of DZs, but they do not completely cover the surface, so $A_{nuc} > 0$. We simultaneously nucleated islands at random locations in the region outside all DZs, as well as along the CZ boundaries formed by colliding DZs. This makes for a smoother transition between the distinct prescriptions of nucleation in the transient and steady-state regimes. However, we find that a direct transition is sufficient if chosen close to θ^*.

(iii) In the steady-state regime, nucleation occurs precisely on CZ boundaries in the simplest GBS algorithm described above. This algorithm has proved successful in accurately predicting island size and CZ area distributions but less effective in predicting spatial correlations between island positions [33, 34]. However, a simple refinement involving suitably distributing nucleation positions off CZ boundaries can resolve this shortcoming [33, 34].

Appendix B. Nucleation rate in "point-island" models for small *i*. To test the ideas developed in sections 3.1 and 3.2, it is natural to consider modified models still with $E_i = 0$ but where different behavior is expected. To this end, we consider a "point-island"-type model, where adatoms in unstable clusters are completely noninteracting in the sense that more than one adatom can occupy the same site. Specifically, adatoms can hop to any neighboring site at rate h, provided they are not on a site containing i or more other adatoms. When $i+1$ adatoms first occupy a single site, a new stable island is nucleated irreversibly on that site. When additional adatoms reach that site, either by diffusion or direct deposition, they are irreversibly incorporated into the island, which still occupies a single site (but for which a size counter is maintained to track its size). For this model, it is clear that the prefactor in the Walton relation is given by $c_i = 1$ for all i. Correspondingly, the nucleation rate for $i > 1$ should be greatly reduced from that for the canonical model. Simulation results confirm this picture. See Figure B.1.

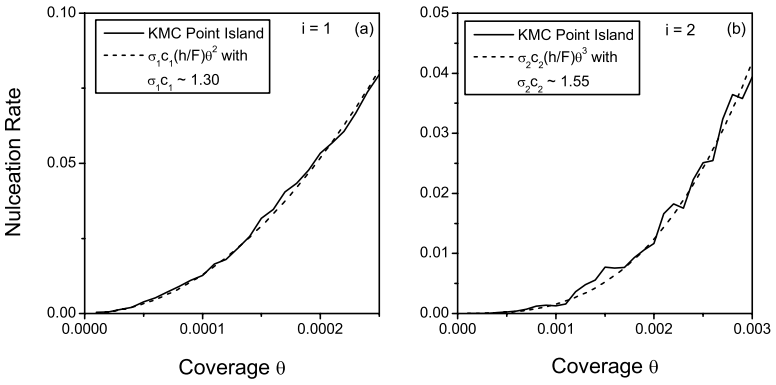

FIG. B.1. *Initial nucleation rate for the "point-island" model with $i = 1$ and 2 and $h/F = 10^6$. The best fit values for $c_i\sigma_i$ are also indicated.*

Appendix C. Island size distribution at crossover for large i. In the simplest treatment island growth in the transient regime, one simply tracks the nucleation coverages, $\theta_{nuc} = Ft_{nuc}$, of various islands, sets $\delta\theta = \theta^* - \theta_{nuc}$, and then assigns sizes, $S \approx \pi(h/F)(\delta\theta_{nuc})^2/2$, at θ^*. An understanding of the island size distribution at θ^* comes from the recognition that the population, N_s^*, of islands of a certain size, s, is proportional to the nucleation rate at that prior time which would produce islands of size s at θ^*. Then using (2.3) for the nucleation rate with $q = i + 1$, and setting $S_{max}^* \approx \pi(h/F)(\theta^*)^2/2$, it follows that $N_s^* \propto (S_{max}^*)^{-1}[1 - (s/S_{max}^*)^{1/2}]^{i+1}$ for $s < S_{max}^*$ (and 0 otherwise).

REFERENCES

[1] Z. Zhang and M. G. Lagally, eds., *Morphological Organization in Epitaxial Growth and Removal*, World Scientific, Singapore, 1997.

[2] T. Michely and J. Krug, *Islands, Mounds, and Atoms*, Springer-Verlag, Berlin, 2003.

[3] G. Zinsmeister, *Theory of thin film condensation. Part B: Solution of the simplified condensation equation*, Thin Solid Films, 2 (1969), pp. 497–507; *Theory of thin film condensation Part D: Influence of a variable collision factor*, Thin Solid Films, 7 (1971), pp. 51–75.

[4] J. A. Venables, *Rate equation approaches to thin film nucleation kinetics*, Phil. Mag., 27 (1973), pp. 697–738.

[5] M. C. Bartelt and J. W. Evans, *Scaling analysis of diffusion-mediated island growth in surface adsorption processes*, Phys. Rev. B, 46 (1992), pp. 12675–12687.

[6] M. C. Bartelt and J. W. Evans, *Nucleation and growth of square islands during deposition: Sizes, coalescence, separations and correlations*, Surf. Sci., 298 (1993), pp. 421–431.

[7] J. W. Evans and M. C. Bartelt, *Nucleation and growth in metal-on-metal homoepitaxy: Rate equations, simulations and experiments*, J. Vac. Sci. Technol. A, 12 (1994), pp. 1800–1808.

[8] G. S. Bales and D. C. Chrzan, *Dynamics of irreversible island growth during submonolayer epitaxy*, Phys. Rev. B, 50 (1994), pp. 6057–6067.

[9] M. C. Bartelt and J. W. Evans, *Exact island-size distributions for submonolayer deposition: Influence of correlations between island size and separation*, Phys. Rev. B, 54 (1996), pp. 17359–17362.

[10] M. C. Bartelt, A. K. Schmid, J. W. Evans, and R. Q. Hwang, *Island size and environment dependence of adatom capture: Cu/Co islands on Ru(*0001*)*, Phys. Rev. Lett., 81 (1998), pp. 1901–1904.

[11] M. C. Bartelt, C. R. Stoldt, C. J. Jenks, P. A. Thiel, and J. W. Evans, *Adatom capture by arrays of two-dimensional Ag islands on Ag(*100*)*, Phys. Rev. B, 59 (1999), pp. 3125–3134.

[12] D. D. Vvedensky, R. E. Caflisch, M. F. Gyure, B. Merriman, S. Osher, C. Ratsch, and J. J. Zink, *Island size distributions in submonolayer epitaxy: Rate equations and beyond*, MRS Proc., 528 (1998), pp. 261–274.

[13] R. E. Caflisch, M. F. Gyure, B. Merriman, S. Osher, C. Ratsch, D. D. Vvedesnky, and J. J. Zink, *Island dynamics and level set methods for continuum modeling of epitaxial growth*, Appl. Math. Lett., 12 (1999), pp. 13–22.

[14] C. Ratsch, M. F. Gyure, S. Chen, M. Kang, and D. D. Vvedensky, *Fluctuations and scaling in aggregation phenomena*, Phys. Rev. B, 61 (2000), pp. 10598–10601.

[15] M. Petersen, C. Ratsch, R. E. Caflisch, and A. Zangwill, *Level set approach to reversible epitaxial growth*, Phys. Rev. E (3), 64 (2001), 061602.

[16] C. Ratsch, M. F. Gyure, R. E. Caflisch, M. Petersen, M. Kang, J. Garcia, and D. D. Vvedensky, *Level-set method for island dynamics in epitaxial growth*, Phys. Rev. B, 65 (2002), 195403.

[17] T. P. Schulze and W. E, *A continuum model for the growth of epitaxial films*, J. Crystal Growth, 222 (2001), pp. 414–425.

[18] T. P. Schulze, P. Smereka, and W. E, *Coupling kinetic Monte-Carlo and continuum models with application to epitaxial growth*, J. Comput. Phys., 189 (2003), pp. 197–211.

[19] E. Bansch, P. Morin, and R. H. Nochetto, in Proc. Int. Conf. on Free Boundary Problems: Theory and Applic., Trento, Italy, 2002.

[20] R. E. Caflisch and B. Li, *Analysis of island dynamics in epitaxial growth of thin films*, Multiscale Model. Simul., 1 (2003), pp. 150–171.

[21] E. Bansch, F. Hausser, O. Lakkis, B. Li, and A. Voigt, *Finite element method for epitaxial growth with attachment-detachment kinetics*, J. Comput. Phys., 194 (2004), pp. 409–434.

[22] W. K. Burton, N. Cabrera, and F. C. Frank, *The growth of crystals and the equilibrium structure of their surfaces*, Philos. Trans. Roy. Soc. London Ser. A, 243 (1951), pp. 299–358.
[23] J. A. Venables and D. J. Ball, *Nucleation and growth of rare-gas crystals*, Proc. Roy. Soc. A, 322 (1971), pp. 331–354.
[24] P. A. Mulheran and J. A. Blackman, *Capture zones and scaling in homogeneous thin-film growth*, Phys. Rev. B, 53 (1996), pp. 10261–10267.
[25] T. Witten and L. M. Sander, *Diffusion-limited aggregation, a kinetic critical phenomenon*, Phys. Rev. Lett., 47 (1981), pp. 1400–1403.
[26] J. W. Evans, *Analysis of a diffusion-limited island growth mechanism for chemisorption and epitaxy*, Phys. Rev. A, 40 (1989), pp. 2868–2870.
[27] M. A. Petersen, *Singular Laplacian growth*, Phys. Rev. E (3), 57 (1998), pp. 3221–3226.
[28] G. S. Bales and A. Zangwill, *Morphological instability of a terrace edge during step-flow growth*, Phys. Rev. B, 41 (1990), pp. 5500–5508.
[29] L. Mandreoli, J. Neygebauer, R. Kunert, and E. Scholl, *Adatom density kinetic Monte Carlo: A hybrid approach to perform epitaxial growth simulations*, Phys. Rev. B, 68 (2003), 155429.
[30] G. Russo, L. M. Sander, and P. Smereka, *Quasicontinuum Monte Carlo: A method for surface growth simulations*, Phys. Rev. B, 69 (2004), 121406.
[31] C. Ratsch, J. Garcia, and R. E. Caflisch, *The influence of edge diffusion on the growth of vicinal surfaces*, Bull. Am. Phys. Soc., 48 (2003), p. 257.
[32] M. Li and J. W. Evans, *Growth coalescence shapes for islands during metal (*100*) homoepitaxy*, Phys. Rev. B, 69 (2004), 035410.
[33] M. Li, M. C. Bartelt, and J. W. Evans, *Geometry-based simulation of submonolayer film growth*, Phys. Rev. B, 68 (2003), 121401.
[34] M. Li and J. W. Evans, *Geometry-based simulation (GBS) algorithms for island nucleation and growth during sub-monolayer deposition*, Surf. Sci., 546 (2003), pp. 127–148.
[35] G. Ehrlich and F. G. Hudda, *Atomic view of surface diffusion-tungsten on tungsten*, J. Chem. Phys., 44 (1966), pp. 1039–1049.
[36] R. L. Schwoebel and E. J. Shipsey, *Step motion on crystal surfaces*, J. Appl. Phys., 37 (1996), p. 3682.
[37] K. J. Caspersen, D. J. Liu, M. C. Bartelt, C. R. Stoldt, A. R. Layson, P. A. Thiel, and J. W. Evans, *Nanostructure formation and relaxation in metal(*100*) homoepitaxial thin films: Atomistic and continuum modeling*, in Models and Applications of Computational Materials Chemistry, L. A. Curtiss and M. S. Gordon, eds., Kluwer, Dordrecht, The Netherlands, 2004, pp. 91–120.
[38] L.-H. Tang, *Island formation in submonolayer epitaxy*, J. Phys. I (France), 3 (1993), pp. 935–950.
[39] B. D. Hughes, *Random Walks and Random Environments; Vol.* 1 *Random Walks*, Clarendon, Oxford, UK, 1995.
[40] H. B. Rosenstock, *Random walks with spontaneous emission*, J. Soc. Indust. Appl. Math., 9 (1961), pp. 169–188.
[41] J. W. Evans, *Random and cooperative sequential adsorption*, Rev. Modern Phys., 65 (1993), pp. 1281–1329.
[42] P. Griffin, *Accelerating beyond the third dimension: Returning to the origin in simple random walk*, Math. Scientist, 15 (1990), pp. 24–35.
[43] A. Pimpinelli and J. Villain, *Physics of Crystal Growth*, Cambridge University Press, Cambridge, UK, 1998.
[44] P. Jensen, H. Larralde, and A. Pimpinelli, *Effect of monomer evaporation on a simple model of submonolayer growth*, Phys. Rev. B, 55 (1997), pp. 2556–2569.
[45] M. Avrami, *Kinetics of phase change* I *General theory*, J. Chem. Phys., 7 (1939), pp. 1103–1112; *Kinetics of phase change* II *Transformation-time ralations for random distribution of nuclei*, J. Chem. Phys. 8 (1940), pp. 212–224; *Granulation, phase change, and microstructure. Kinetics of phase change* III, J. Chem. Phys., 9 (1941), pp. 177–184.
[46] P. A. Mulheran, *Island statistics reflecting growth processes*, in Atomistic Aspects of Epitaxial Growth, M. Kotrla, N. I. Papanicolaou, D. D. Vvedensky, and L. T. Wille, eds., Kluwer, Dordrecht, The Netherlands, 2002, p. 111.
[47] G. Haas, A. Menck, H. Brune, J. V. Barth, J. A. Venables, and K. Kern, *Nucleation and growth of supported clusters at defect sites: Pd/MgO(*001*)*, Phys. Rev. B, 61 (2000), pp. 11105–11108.
[48] V. Fournee, A. R. Ross, T. A. Lograsso, J. W. Evans, and P. A. Thiel, *Growth of Ag thin films on complex surfaces of quasicrystals and approximant phases*, Surf. Sci., 537 (2003), pp. 5–26.

[49] P. A. Mulheran and J. A. Blackman, *Capture zones and scaling in thin film growth*, Philos. Mag. Lett., 72 (1995), pp. 55–60.
[50] D. D. Chambliss and K. E. Johnson, *Nucleation with a critical cluster size of zero: Submonolayer Fe inclusions in Cu(*100*)*, Phys. Rev. B, 50 (1994), pp. 5012–5015.
[51] J. Villain, A. Pimpinelli, L. Tang, and D. Wolf, *Terrace sizes in molecular beam epitaxy*, J. Phys. I (France), 2 (1992), pp. 2107–2121.
[52] S. Liu, L. Bonig, and H. Metiu, *Effect of small-cluster mobility and dissociation on the island density in epitaxial growth*, Phys. Rev. B, 52 (1995), pp. 2907–2913.
[53] M. C. Bartelt, S. Gunther, E. Kopatzki, R. J. Behm, and J. W. Evans, *Island-size distributions in submonolayer epitaxial growth: Influence of the mobility of small clusters*, Phys. Rev. B, 53 (1996), pp. 4099–4104.
[54] J. W. Evans and M. C. Bartelt, *Submonolayer nucleation and growth of islands and multilayer mound formation during homoepitaxy*, in Morphological Organization in Epitaxial Growth and Removal, Z. Zhang and M. G. Lagally, eds., World Scientific, Singapore, 1997, pp. 50–72.
[55] P. A. Mulheran and D. A. Robbie, *Theory of the island and capture zone size distributions in thin film growth*, Europhys. Lett., 49 (2000), pp. 617–623.
[56] J. G. Amar, M. N. Popescu, and F. Family, *Rate-equation approach to island capture zones and size distributions in epitaxial growth*, Phys. Rev. Lett., 86 (2001), pp. 3092–3095.
[57] M. N. Popescu, J. G. Amar, and F. Family, *Rate-equation approach to island size distributions and capture numbers in submonolayer irreversible growth*, Phys. Rev. B, 64 (2001), 205404.
[58] A. Zangwill, *Advances in aggregation*, Nature, 411 (2001), pp. 651–652.
[59] J. W. Evans and M. C. Bartelt, *Nucleation, adatom capture, and island size distributions: Unified scaling analysis for submonolayer deposition*, Phys. Rev. B, 63 (2001), 235408.
[60] J. W. Evans and M. C. Bartelt, *Island sizes and capture zone areas in submonolayer deposition: Scaling and factorization of the joint probability distribution*, Phys. Rev. B, 66 (2002), 235410.